Copy 210
RM L52K20

NACA RM L52K20

RESEARCH MEMORANDUM

SUMMARY OF PITCH-DAMPING DERIVATIVES OF COMPLETE AIRPLANE AND MISSILE CONFIGURATIONS AS MEASURED IN FLIGHT AT TRANSONIC AND SUPERSONIC SPEEDS

By Clarence L. Gillis and Rowe Chapman, Jr.

Langley Aeronautical Laboratory
Langley Field, Va.

NATIONAL ADVISORY COMMITTEE
FOR AERONAUTICS

WASHINGTON
January 22, 1953

NATIONAL ADVISORY COMMITTEE FOR AERONAUTICS

RESEARCH MEMORANDUM

SUMMARY OF PITCH-DAMPING DERIVATIVES OF COMPLETE AIRPLANE AND MISSILE CONFIGURATIONS AS MEASURED IN FLIGHT AT TRANSONIC AND SUPERSONIC SPEEDS

By Clarence L. Gillis and Rowe Chapman, Jr.

SUMMARY

Longitudinal-damping data in the form of the pitching-moment damping derivatives $\left(C_{m_q} + C_{m_{\dot{\alpha}}}\right)$ are presented and summarized from NACA flight tests of rocket-propelled models and full-scale airplanes. The experimental data are compared with calculations and a discussion of each configuration is given. Detailed conclusions are precluded by the lack of systematic configuration changes and the relatively unknown effects of various factors. A general comparison of the results revealed the following trends and general conclusions. The contribution to the pitch-damping derivatives of wings having 45° or less sweepback is erratic in the transonic region and may be either positive or negative, leading to possible dynamic instability of tailless configurations using such wings. No satisfactory method of calculating the damping of such wings in the transonic region is available and a smoothly faired curve between subsonic and supersonic calculated values will probably be unconservative. Configurations having triangular and swept wings with approximately 60° leading-edge sweep and rounded airfoil sections exhibited less variation in damping in the transonic region. Calculated values of the pitch-damping derivatives for configurations with horizontal tails are more conservative and give better agreement with experimental results if the distance from the trailing edge of the wing mean aerodynamic chord (instead of from the center of gravity) to the tail is used to calculate the downwash lag effect. The damping caused by downwash effects arising from lift on a forward surface due to pitching velocity and rate of change of angle of attack may be appreciable if the forward surface is at a large distance from the center of gravity.

INTRODUCTION

Successful accomplishment of aircraft flight at transonic and supersonic speeds has served to place increased emphasis on the dynamic behavior of aircraft. The type of behavior referred to here concerns motions of the aircraft as a whole as compared to motions of component parts usually referred to as flutter. Dynamic instability of the lateral and directional modes of motion is a problem that has occupied the designer's attention for some time. A trend toward deterioration of the damping of the longitudinal motion of aircraft operating in the transonic region has also been experienced. This decrease in damping, as measured by cycles to damp, occurs because of the high altitude at which such flights are usually conducted and because of an actual decrease in the dimensionless aerodynamic damping-in-pitch derivatives at transonic speeds for some aircraft configurations (refs. 1 and 2).

The present paper summarizes the available experimental data obtained by the National Advisory Committee for Aeronautics on pitch-damping derivatives measured in flight at transonic and low supersonic speeds. Most of the data contained herein were obtained from rocket-propelled models of airplane or missile configurations flown at the Langley Pilotless Aircraft Research Station at Wallops Island, Va. Some data are also shown for several piloted airplanes obtained from flights at Ames Aeronautical Laboratory and the NACA High-Speed Flight Research Station at Edwards, Calif.

Some of the damping information presented herein has been published previously as parts of general longitudinal-stability investigations and some is, as yet, unpublished. In the present paper the damping data are compared with each other and with values calculated by the usual methods.

SYMBOLS

C_L	lift coefficient, L/qS
C_m	pitching-moment coefficient, $\frac{\text{Pitching moment}}{qS\bar{c}}$
A	aspect ratio
C	constant in stability equation
I_Y	mass moment of inertia about Y-axis, slug-ft^2
k_Y	radius of gyration in pitch, $\sqrt{I_Y/m}$, ft

L	lift
M	Mach number
S	wing area (including area enclosed within fuselage), sq ft
S_t	horizontal-tail area (total included area), sq ft
V	forward velocity, ft/sec
W	weight of body, lb
b	wing span in equation for $\bar{c}$, ft
b	damping constant in stability equations
c	local chord, ft
$\bar{c}$	mean aerodynamic chord, $\frac{2}{S}\int_0^{b/2} c^2\,dy$, ft
g	acceleration due to gravity, ft/sec^2
l	tail length, measured from center of gravity of configuration to center of pressure of tail, ft
m	mass of body, W/g, slugs
p	free-stream static pressure, lb/sq ft
q	dynamic pressure when used in equations for C_L and C_m and equations (2) and (3), $\frac{1}{2}\gamma pM^2$, lb/sq ft
$q = \frac{d\theta}{dt}$	
t	time, sec
Y	reference axis through center of gravity of configuration perpendicular to plane of symmetry
α	angle of attack, radians
γ	specific heat ratio (1.40)
δ	control-surface deflection, deg

ϵ	angle of downwash, radians
θ	angle of pitch, radians
$\dot{\alpha}$	rate of change of angle of attack, $d\alpha/dt$
φ	phase angle, radians
ω	frequency of oscillation, radians/sec

$$C_{m_q} = \frac{dC_m}{d\left(\frac{q\bar{c}}{2V}\right)}$$

$$C_{m_{\dot{\alpha}}} = \frac{dC_m}{d\left(\frac{\dot{\alpha}\bar{c}}{2V}\right)}$$

$$C_{L_q} = \frac{dC_L}{d\left(\frac{q\bar{c}}{2V}\right)}$$

$$C_{L_{\dot{\alpha}}} = \frac{dC_L}{d\left(\frac{\dot{\alpha}\bar{c}}{2V}\right)}$$

$$C_{L_\alpha} = \frac{dC_L}{d\alpha}$$

Subscripts:

f	forward surface, based on its own area and chord
r	rear surface, based on its own area and chord
t	tail
T	trimmed, or mean value

TEST AND ANALYSIS PROCEDURE

Experimental data presented were obtained in free flight by the free-oscillation technique. In this test method, the aircraft is disturbed from a trimmed condition, usually by means of a rapid elevator deflection and the resulting short-period oscillation is recorded as the elevator is held fixed. The method of analysis of these oscillations to obtain the static and dynamic stability derivatives is adequately covered in several references (such as ref. 3). For the present purpose, only that portion of the procedure dealing with the pitch-damping derivatives is of interest.

Making the usual assumptions of constant velocity, level flight, and linear aerodynamic derivatives, a solution of the two-degrees-of-freedom equation of longitudinal motion of an aircraft can be obtained. For any appropriate quantity such as normal acceleration or angle of attack, the solution is of the form

$$\alpha = Ce^{bt}\cos(\omega t + \varphi) + \alpha_T \tag{1}$$

The constant b in equation (1) defines the damping of an oscillation and in terms of the aerodynamic derivatives is given by

$$b = -\frac{Sq}{2m\bar{V}}\left[C_{L_\alpha} - \frac{1}{2}\left(C_{m_q} + C_{m_{\dot{\alpha}}}\right)\left(\frac{\bar{c}}{k_Y}\right)^2\right] \tag{2}$$

Equation (2) may be solved for the sum of the damping derivatives to give

$$C_{m_q} + C_{m_{\dot{\alpha}}} = \frac{4I_Y}{Sq\bar{c}^2}\left(b + \frac{Sq}{2m\bar{V}}\,C_{L_\alpha}\right) \tag{3}$$

From the flight tests, therefore, the sum of the damping derivatives C_{m_q} and $C_{m_{\dot{\alpha}}}$ may be determined if the damping constant b is measured and the lift-curve slope C_{L_α} is known. The damping factor b is generally determined from the envelope of the curve defined by equation (1). This envelope is determined from the flight record of the appropriate measured quantity which, for rocket models, is angle of attack. The equation for the damping factor is

$$b = \frac{\log_e \Delta\alpha_2/\Delta\alpha_1}{t_2 - t_1} \tag{4}$$

where $\Delta\alpha_1$ and $\Delta\alpha_2$ are the amplitudes measured from the mean value of α at times t_1 and t_2. For rocket-model tests, normal acceleration and angle of attack were measured to provide the lift-curve slopes. In some cases for the full-scale airplane tests reliable angle-of-attack information was not available from the flight test so the lift-curve slope was obtained from wind-tunnel tests and equations (1) and (4) would be written in terms of the lift coefficient. The test and analysis method described does not permit separation of the derivatives C_{m_q} and $C_{m_{\dot{\alpha}}}$. This is not a severe limitation, however, because the damping is always proportional to the sum of the two derivatives regardless of the flight conditions or mass characteristics.

In free-flight tests, accurate measurement of the damping derivative $\left(C_{m_q} + C_{m_{\dot{\alpha}}}\right)$ is difficult for several reasons. First, as shown by equation (2), the total damping is composed of the damping-derivative term and the lift-curve slope term, the relative magnitudes of which depend on the radius of gyration in pitch. The inaccuracies in $C_{m_q} + C_{m_{\dot{\alpha}}}$, as obtained by solution of equation (2), are proportional to the relative contribution of the C_{L_α} term to the total damping, b. As an example, the C_{L_α} term contributed as much as two-thirds of the total damping in some of the rocket models, and in a full-scale test of an airplane (ref. 1) the C_{L_α} term contributed about one-half of the total damping. Present design trends indicate that the proportion of damping contributed by the C_{L_α} term on future airplanes will more nearly approach the proportion for the rocket models. Other factors which may contribute to inaccuracies in measuring $C_{m_q} + C_{m_{\dot{\alpha}}}$ are nonlinear aerodynamic derivatives, disturbances due to gusts, and any other effects on the oscillation peaks which define the envelope of the curve. Gusts and nonlinear aerodynamic derivatives usually appear as apparent changes in the damping coefficients.

CALCULATION METHOD

The experimental damping derivatives presented herein are compared with calculated values from theoretical investigations wherever applicable, or experimental test data where such are available. It has frequently been assumed that all the damping on conventional airplane configurations is caused by the tail. A damping moment derivative C_{m_q} results from the additional angle of attack at the tail caused by the velocity of pitching about an axis through the center of gravity. A damping moment derivative $C_{m_{\dot{\alpha}}}$ results from the lag in downwash at the tail surface due to the finite time required for the downwash discharged at the wing to reach the tail surface (ref. 4). The damping derivatives

arising from these concepts are given by the equation

$$\left(C_{m_q} + C_{m_{\dot{\alpha}}}\right)_t = -\left(1 + \frac{d\epsilon}{d\alpha}\right)\left(2\ C_{L_{\alpha_t}}\right)\frac{S_t}{S}\left(\frac{l_t}{\bar{c}}\right)^2 \tag{5}$$

where the downwash lag contribution is represented by the $d\epsilon/d\alpha$ factor in equation (5). A factor such as this assumes that the downwash lag term is characterized by downwash discharged at the center of gravity of the configuration. It appears that this downwash lag term might be more representative if it is assumed that the downwash is discharged at the trailing edge of the mean aerodynamic chord of the wing rather than at the center of gravity. Modification of formula (5) in accordance with this concept gives

$$\left(C_{m_q} + C_{m_{\dot{\alpha}}}\right)_t = -\left(1 + \frac{l'}{l_t}\frac{d\epsilon}{d\alpha}\right)\left(2\ C_{L_{\alpha_t}}\right)\frac{S_t}{S}\left(\frac{l_t}{\bar{c}}\right)^2 \tag{6}$$

where l' is the length from the trailing edge of the mean aerodynamic chord to the center of pressure of the tail.

For airplanes in which the tail contributes the largest part of the damping, equation (6) is satisfactory for an approximate calculation. It obviously fails for a tailless airplane. For airplanes with swept wings the damping contributed by the wing may be of appreciable magnitude at all speeds, and in the transonic region the wing damping may be of primary importance for wings of any plan form. Theoretical studies (refs. 5 to 8) and experimental data (refs. 9 and 10) show that, at transonic and low supersonic speeds, the wing itself may be dynamically unstable. Calculations of the damping derivatives should therefore include the wing even though the damping due to the tail may be the major factor.

Additional increments in damping-moment coefficients arise because of the downwash on a rear lifting surface resulting from the lift on a forward surface produced by the pitching velocity $\left(C_{L_q}\right)$ and the rate of change of angle of attack $\left(C_{L_{\dot{\alpha}}}\right)$. The damping coefficients caused by this effect may be calculated as follows:

$$\Delta C_{m_q} = \frac{d\epsilon}{d\left(\frac{q\bar{c}}{2V}\right)}\frac{dC_m}{d\epsilon} \tag{7}$$

$$\Delta C_{m_q} = \left[\left(\frac{dC_{L_f}}{d\left(\frac{q\bar{c}}{2V}\right)_f}\right)\left(\frac{d\alpha}{dC_{L_f}}\right)\frac{\bar{c}_f}{\bar{c}}\left(\frac{d\epsilon}{d\alpha}\right)\right]\left(C_{L_{\alpha_r}}\frac{l_r}{\bar{c}}\frac{S_r}{S}\right) \tag{8}$$

where S and $\bar{c}$ are the quantities on which C_m is based. A similar expression can be derived for $\Delta C_{m_{\dot{\alpha}}}$. The sum of the two damping-moment coefficients is then:

$$\Delta\left(C_{m_q} + C_{m_{\dot{\alpha}}}\right) = \left(\frac{C_{L_{\alpha_r}}}{C_{L_{\alpha_f}}} \frac{l_r}{\bar{c}} \frac{S_r}{S} \frac{\bar{c}_f}{\bar{c}} \frac{d\epsilon}{d\alpha}\right)\left(C_{L_{q_f}} + C_{L_{\dot{\alpha}_f}}\right) \tag{9}$$

As will be shown later this increment in the damping derivatives is very small for conventional airplane configurations but can be fairly large for canard configurations. If the forward lifting surface is at a large distance from the center of gravity, the quantity $\frac{d\epsilon}{d\left(\frac{q\bar{c}}{2V}\right)}$ can be obtained to a close approximation by the expression

$$\frac{d\epsilon}{d\left(\frac{q\bar{c}}{2V}\right)} = \frac{2l_f}{\bar{c}} \frac{d\epsilon}{d\alpha}$$

The theoretical results used to calculate the pitch-damping derivatives for subsonic and supersonic speeds are given in references 5 to 8, 11, and 12. References 5 and 11 consider only untapered wings but the results were assumed to apply to tapered wings also. Wherever possible, wind-tunnel measurements of tail effectiveness and downwash were used to calculate the damping caused by the tail.

In calculating the derivative $C_{m_{\dot{\alpha}}}$ the simple downwash lag concept as given in equation (5) and modified in equation (6) was used at all speeds. Several refinements to these calculations have been considered in references 13 and 14 but for the present purpose these refinements were neglected because of the uncertainties in the experimental results caused by large possible experimental errors in some cases and the relatively unknown but important effects of oscillation amplitude.

RESULTS AND DISCUSSION

The results of the flight measurements and the calculations are shown in figures 1 to 25 for airplane and missile configurations. All information pertaining to one configuration is given in one figure; break lines on the drawings of the models indicate wedge and hexagonal airfoil sections. The details of the airfoil section for each model are given in table I. For consistency, damping coefficients in all figures are based on the total area and mean aerodynamic chord of the wing and are given for the rate terms (q and $\dot{\alpha}$) in radians per second. This method of presentation does not correspond to that of the references from which the data were taken for some cases.

Scales to which the derivatives $(C_{m_q} + C_{m_{\dot{\alpha}}})$ are plotted vary considerably between figures. It is important to note, as pointed out in reference 15, that a comparison of the absolute values of damping coefficients for different configurations has little significance. When presented, the curve designated "calculated (tail)" is the value obtained from equation (6), using wind-tunnel values of $C_{L_{\alpha_t}}$ and $d\epsilon/d\alpha$. The calculated (tail) curve thus includes the downwash lag effect which is an indirect effect of the wing but acts on the tail. The direct damping of the wing, calculated from theoretical results for the conventional airplane configurations was added to the calculated (tail) curve to give the curve designated "calculated (tail plus wing)." For the canard configurations, the calculated curve includes the damping increments given by equation (9) and the theoretical values of $C_{m_{\dot{\alpha}}}$ given by references 5 and 6. There are insufficient data available to permit estimation of the effects of airfoil shape, oscillation amplitude, or oscillation frequency. Reference 16 shows some effects of oscillation amplitude and frequency on the damping derivatives $(C_{m_q} + C_{m_{\dot{\alpha}}})$ for a 45° delta wing at subsonic speeds For reference, table II gives the reduced-frequency range for all models, and it may be noted that the frequency ranges for most of the data discussed herein are below the ranges investigated in reference 16.

Rocket-Propelled Models

Model 1.- The experimental data for model 1 are contained in reference 17 and, as shown in figure 1, exhibit a smooth variation through the transonic region. Theoretical values of $C_{m_q} + C_{m_{\dot{\alpha}}}$ and $C_{m_{\dot{\alpha}}}$ are also shown in figure 1 for the pertinent supersonic speeds. The positive value of $C_{m_{\dot{\alpha}}}$ at supersonic speeds decreases the C_{m_q} damping of the wing by approximately one-third. Although the experimental curve is considerably higher than the theoretical curve, the variations with Mach number are similar. The effect of the fuselage was investigated by the use of reference 18, which does not include the effect of the afterbody, and was found to be negligible. No data are available on the effects of the afterbody.

Model 2.- Figure 2 shows the experimental data for two models of a tailless airplane configuration. The data for model 2 were taken from unpublished rocket-test results. No curve is faired since the data were at isolated Mach numbers and were obtained from sustained low-amplitude oscillations ($\Delta\alpha \approx \pm 0.25°$) at $M = 0.91$ and 1.24. The oscillation amplitude for the points at $M = 1.34$ was $\Delta\alpha \approx \pm 1.0°$.

Model 2B (data previously unpublished) contained pulse rockets to disturb the model and, therefore, higher angles of attack were obtained in the test. The data obtained at higher angles of attack ($\Delta\alpha \approx \pm 1.0°$)

confirmed the data for model A at $M = 1.34$, which was for similar angle-of-attack variations. Model B also exhibited a continued oscillation of low amplitude ($\pm 0.25^\circ$) similar to that which gave the positive damping coefficients for model A. Analysis of these low-amplitude oscillations, assuming time to damp to one-half amplitude as infinite, gave values of $C_{m_q} + C_{m_{\dot{\alpha}}}$ as varying from 1.98 to 2.25. The values of damping obtained at higher amplitudes shown by the data points for model B and low amplitudes shown by positive data points for model A are in reality boundaries for the damping coefficients where the coefficients for the system depends with certainty on the amplitude of the oscillation and possibly on the value of the mean angle of attack.

In order to calculate the theoretical damping it was necessary to approximate the actual wing plan form by one more amenable to calculation. Three approximations were tried: a swept tapered wing obtained by extending the leading and trailing edges to the root and tip, a triangular wing having the same aspect ratio as the actual wing, and a triangular wing having the same leading-edge sweep as the actual wing. The calculated curves are shown for all three approximations and best agreement was obtained between the calculated 52.5° triangular wing and the flight data.

Model 3.- Data are presented in figure 3 for two tailless models designed to have different wing flexibilities. These data are from a program instituted to investigate the effects of wing flexibility on longitudinal stability. The solid line (model A) in figure 3 is experimental data for a 9-percent-thick wing of laminated wood and metal construction having medium rigid characteristics and is labeled "least flexible wing." The dashed line is for a wing having the same geometric shape and thickness but with thinner metal inserts, hence, model B had a more flexible wing and is labeled "flexible wing." The least flexible wing had a stiffness of approximately one-half that of a solid aluminum wing of the same thickness and the flexible wing had a stiffness of approximately one-third that of a solid aluminum wing of the same thickness. These stiffness ratios were determined by comparison of the influence coefficients for the solid aluminum wing and the laminated wing.

A calculation of the C_{m_q} damping of the wing was made at $M = 0.7$ by the method of reference 11. The subsonic calculation gave the value of C_{m_q} as approximately -16, which is far too high and unconservative when compared with the experimental data. It is possible that the disagreement between calculation and experiment at subsonic speeds may be due to a positive $C_{m_{\dot{\alpha}}}$ for the wing which is not accounted for in the computation. A computation of damping at $M = 1.414$ was made by using references 7 and 8 and good agreement with the experimental data was obtained.

Model 4.- Unpublished data for a 45° swept-wing tailless configuration are shown in figure 4. The wing was a 6-percent-thick section constructed of solid dural. Qualitatively, the shape of the curves for damping of models 3A, 3B, and 4 show remarkable similarity for Mach numbers from 0.90 to 1.15 with damping for both models exhibiting a characteristic drop in this region. The wing on model 4 was comparable in stiffness to the flexible wing of model 3. Data for model 4 were not obtained below a Mach number of 0.88; hence, it is not known if the damping decreased in a manner similar to that for model 3. One calculated point for the wing alone is shown at a Mach number of 1.38. The calculated value is conservative but shows poor agreement with the experimental data. A calculation of body damping by the use of reference 19 showed the body contribution to be small at supersonic speeds because of the afterbody shape.

Model 5.- The data for model 5 (fig. 5) are from reference 20. This model was a wingless fuselage-tail configuration that has been used for tests of a number of wing plan forms for supersonic airplanes (models 6 to 12). The damping coefficients in figure 5 are based on the wing area and chord of model 6 for comparison purposes. The theoretical values of $C_{m_q} + C_{m_{\dot{\alpha}}}$ agree fairly well with the experimental values, particularly at supersonic speeds, as does the calculated values of C_{m_q} of the tail surface (curve labeled "calculated C_{m_q} (tail)"). The agreement of the theoretical and experimental values is somewhat fortuitous, however, because, as shown in figure 5, the theoretical values of C_{m_q} are considerably higher than those calculated from measured values of tail effectiveness. The theoretical values of $C_{m_{\dot{\alpha}}}$, which are those for the isolated tail uninfluenced by downwash, are positive throughout the supersonic speed range considered and become rapidly larger as the Mach number decreases below about 1.2.

Model 6.- The data for model 6 (fig. 6) are from reference 20. Two geometrically identical models were flown; model B having a steel wing (designated "rigid wing" in fig. 6) and model A, having an aluminum wing (designated "flexible wing" in fig. 6). At transonic Mach numbers rather large changes in the experimental damping data occurred as contrasted to the smooth variation with Mach number of wing-off data (fig. 5) and calculated tail contribution. As indicated by the calculated curve including the direct wing effects, part of the loss in damping near $M = 1.0$ can be explained by a large positive value of $C_{m_q} + C_{m_{\dot{\alpha}}}$ for the wing. This large destabilizing effect of the wing is caused by the positive value of $C_{m_{\dot{\alpha}}}$ being much larger than the negative value of C_{m_q}. Another reason for the large damping changes near $M = 1.0$ can probably be found in unaccounted-for downwash changes in this region. In calculating the $C_{m_{\dot{\alpha}}}$ portion of the tail contribution to damping it was assumed, in the absence of appropriate data, that the downwash variation with Mach number was similar to the variation of lift-curve slope, which

did not show large changes (ref. 20). Since large changes in static stability for this configuration took place in the transonic region (ref. 20), it is probable that the downwash variation with Mach number was considerably different from that assumed.

The increment in $C_{m_q} + C_{m_{\dot{\alpha}}}$ caused by the downwash resulting from the C_{L_q} and $C_{L_{\dot{\alpha}}}$ on the wing was calculated for model 6 and is shown in figure 6. This contribution to the damping is very small because the terms C_{L_q} and $C_{L_{\dot{\alpha}}}$ are very small and, at least for supersonic speeds, are of opposite sign. Since this condition should be approximately the same for all configurations having the forward surface near the center of gravity, this contribution to the damping was neglected for all other such configurations herein.

Model 7.- Model 7 was identical to model 6 except that the wing had an NACA 65(06)A004.5 airfoil section instead of the sharp-edge hexagonal section on model 6. Data for model 7 are shown in figure 7 and were taken from unpublished data. Model 7, which had an aluminum wing, showed less damping than does model 6A and a larger disagreement between the low-lift experimental curve and the calculated curve for the tail. The reason for the disagreement in the three sets of experimental data has not been established.

Model 8.- Two experimental curves (fig. 8) were obtained for model 8 (ref. 21): one at low lift coefficients and one at high lift coefficients. The calculated tail damping shows a large decrease at Mach numbers near 0.93, as did the test data, and this is caused by the large decrease in downwash at these Mach numbers (ref. 22). The direct effect of the wing was fairly small in the region where it could be calculated. The direct contribution of the wing (as computed) is destabilizing at the supersonic speeds of the test. It is perhaps significant that when the effect of the wing is included, the variations with Mach number of the experimental and calculated curves are, in general, similar at supersonic speeds.

Model 9.- The damping data for two 45° swept-wing models are presented in figure 9 and are not previously published. Model A had a steel wing and is denoted as "rigid wing" in the figure. Model B had an aluminum wing and the curve is labeled "flexible wing" in figure 9. Calculated values of the damping shown for models A and B are based on experimental tail effectiveness. An additional curve labeled "calculated (tail, theoretical)" is shown in the figure and is based on theoretical tail effectiveness. The direct wing contribution to damping at pertinent supersonic Mach numbers was small and is not included in the calculated curves. It is noted that the difference in the experimental damping curves for models A and B is in the opposite direction to that difference in the calculated curves for the two models, which is a center-of-gravity effect. A difference such as this might possibly be

explained by a higher $d\epsilon/d\alpha$ for the more rigid wing. Severe changes in downwash for the flexible wing might explain the high peak and rapid change that occurs between Mach numbers of 0.93 and 1.03 for the flexible wing. Peak values and severe changes such as these occur on a swept-wing airplane which is discussed in a subsequent section.

Model 10.- The data for a 60° swept wing model are shown in figure 10 as obtained from reference 23. The direct contribution of the wing to the total damping is illustrated by the increment between the total damping curve and the tail-damping curve (includes downwash lag). Two additional curves are shown in the figure to illustrate different techniques of computation. The curve labeled "calculated (tail, theoretical)" uses theoretical tail effectiveness plus a downwash lag term from estimated downwash. The peak value of damping which occurs at $M = 0.85$ is not predicted by the calculations but is similar to a peak that occurs in the data of model 11.

Model 11.- The experimental data presented in figure 11 for model 11 are reported in reference 24. This modified triangular-wing model exhibited damping characteristics that showed a marked change between Mach numbers of 0.84 and 0.88 where the damping derivatives almost doubled in value in a manner similar to model 10. Calculated values for the tail and for the tail plus wing are also shown in the figure and show a smooth variation over the Mach number range. The difference in variation between the experimental and calculated curves and a comparison with the data for model 5 indicate that the rise in damping between $M = 0.80$ and $M = 0.90$ can be attributed directly to the wing or to increased downwash from the wing.

Model 12.- The data presented in figure 12 for the 60° triangular-wing model are from reference 25. Two experimental curves are shown in the figure: one for the low-lift-coefficient range and the other for the high-lift-coefficient range. This difference in damping for high and low lift coefficients is primarily attributed to the nonlinear downwash behind the triangular wing. The calculated (low lift, wing plus tail) curve shown is for $d\epsilon/d\alpha$ evaluated at zero lift and for experimental tail effectiveness. Calculated damping coefficients, shown in figure 12, for the wing-plus-tail (high lift) configuration indicate that the increased damping at high lift can be primarily attributed to the increased downwash.

Model 13.- Damping data for a supersonic airplane configuration are shown in figure 13. Experimental data are shown for two models; model A data were at high lift and model B data were at low lift. Curves for tail damping and total damping for model B are also shown in the figure. No computations were made for the high-lift model. The disagreement between the two sets of experimental data at subsonic speeds is believed to be due to the changes in downwash for high and low lift coefficients.

Good agreement was obtained between the computed and experimental data at low lift. From the experimental curve and the fact that it fairs into the calculated (tail plus wing) curve, it appears that the direct wing contribution to damping approaches zero at Mach numbers of approximately 1.17 and 0.90 but generally does not give much destabilizing effect. It is noted that if the calculated (total damping) curve were extended to lower supersonic Mach numbers, the unstable contribution of wing $C_{m_{\dot{\alpha}}}$ would make the agreement between calculation and experiment worse.

Model 14.- Data for a 45° swept-wing airplane model from reference 26 are presented in figure 14. Calculated curves are shown for the tail damping using both the modified and unmodified tail length for the downwash lag term. Flight data vary unpredictably through the transonic region and a comparison with the calculated curve for the tail indicates that the wing contributes both positive and negative damping over the region. A single data point (unpublished) for a similar tailless configuration shows the wing to have a positive (unstable) damping coefficient at $M = 0.79$. The calculated curve using the modified tail-length concept gives better average agreement with the experimental data and is more conservative than the unmodified formula. No total damping calculated curve is shown since the wing contribution was small at the higher Mach numbers where it could be computed and could not be computed over the Mach number range where data were obtained.

Model 15.- The experimental data shown in figure 15 for model 15 were taken from reference 27. A curve of calculated tail damping shows fairly good agreement with the experimental data, both as to magnitude and general variation with Mach number. At subsonic speeds the calculated wing damping was appreciable, being about one-third of that contributed by the tail. For the supersonic speed range below a Mach number of 1.28 the calculated wing damping coefficient is positive and the calculated damping of the complete configuration indicates a greater variation with Mach number than is shown by the experimental data.

Model 16.- Reference 28 and figure 16 contain the experimental data for model 16. Data are presented for models A and B, identical models except for center-of-gravity location. The effect of the center-of-gravity location on the damping is small. In contrast to most other swept-wing configurations included herein, the variation with Mach number of the experimental damping coefficients is smooth and the damping increases as the Mach number increases. The significance of these phenomena and whether they are related to the inverse taper are not known. At subsonic speeds, the calculated wing damping is about 50 percent of that calculated for the tail. Because of the inverse taper ratio on the wing, the methods of references 7 and 8 are not applicable to this model.

Model 17.- The damping data for model 17, shown in figure 17, are from unpublished test results. This model had the same wing as the tailless model 3 and had the same characteristic loss in damping near a Mach number of 1.0. Comparison of the experimental curve for model 17 with the calculated damping of the tail indicates that the wing contributed a positive (unstable) damping coefficient near $M = 1.0$ as did model 3, although the quantitative values of wing damping for models 3 and 17 are not directly comparable because of the different center-of-gravity locations. The agreement of the total calculated damping with the experimental values is very good at subsonic speeds. The wing damping could not be calculated over the supersonic speed range of the tests.

Model 18.- The results shown in figure 18 for a 60° triangular-wing missile configuration are from reference 29. Damping data are presented for both the inline- and interdigitated-tail positions. As pointed out in reference 30 the marked difference in the characteristics for the inline and interdigitated tail can be attributed to the difference in downwash at the tail by considering the rolled-up vortex sheet. The experimental curve for the inline-tail model has a variation with Mach number that is, in general, similar to that for the modified-triangular-wing model (model 11). A calculated curve for the tail is shown as well as a calculated curve for total damping coefficient (both curves being for the inline-tail configuration). Estimates of downwash and tail effectiveness based on experimental data were used and good average agreement with the flight data were obtained. A theoretical curve is shown and is generally nonconservative at the higher Mach numbers but shows good agreement with experimental data in the region near a Mach number of 1.1.

Model 19.- The damping data for a canard missile model shown in figure 19 are unpublished. The calculated damping is considerably less than the experimental damping, but the variation with Mach number of the two curves is remarkably similar. The increments in damping coefficients caused by the downwash resulting from the canard lift effects C_{L_q} and $C_{L_{\dot{\alpha}}}$ were calculated and found to be appreciable as shown in figure 19. This was true for all the canard configurations considered herein. The reason is that the value of C_{L_q} depends upon the distance of a lifting surface from the center of gravity (refs. 5 and 6) and, for the canard surface, becomes fairly large and of the same sign as $C_{L_{\dot{\alpha}}}$, resulting in an appreciable effect on the damping.

Models 20 and 21.- The data for models 20 and 21 were taken from references 31 and 32 and are shown in figure 20. Models 20 and 21 were geometrically identical except that the cylindrical portion of the body between the wing and the canard was 40 inches longer for model 21 than for model 20. All the experimental curves in figure 20 show similar

variations with Mach number near a Mach number of 1.0, which differ considerably from the variations indicated by the calculated curves. For model 21 neither the theoretical damping nor that calculated from experimental data predicted the variation with Mach number of the measured damping at supersonic speeds. The calculated values for model 20 were considerably lower than the experimental values at supersonic speeds but showed a similar variation with Mach number.

Model 22.- The experimental values for model 22 (fig. 21) were taken from unpublished results. Models A and B were identical except for center-of-gravity location and the different lift-coefficient ranges covered by each model. Calculated values exhibit fair agreement with measured values only at supersonic speeds and low lift coefficients. The difference between the calculated values for models A and B was caused partly by the different center-of-gravity locations and partly by different values of downwash (shown by wind-tunnel data) over the two lift-coefficient ranges. Also shown in figure 21 are the values of damping contributed by the downwash resulting from the canard lift effects C_{L_q} and $C_{L_{\dot{\alpha}}}$.

Full-Scale Airplanes

Airplane 1.- Damping data from flight tests of the X-1 research airplane are shown in figure 22. These data were obtained from reference 33, and reference 22 was used to obtain the calculated curves shown on the figure. The calculated damping agrees well with the experimental data both as to magnitude and variation with Mach number. The calculated total damping curve is somewhat lower and agrees better with the experimental data than the calculated curve given in reference 33. This is probably caused by the use herein of the modified tail length for computing the downwash lag effect (eq. (6)). Model 8, previously discussed, was equipped with the X-1 wing. The low-lift experimental data for model 8 show a variation with Mach number very similar to that for the flight-test data of the X-1 airplane.

Airplane 2.- The data for the X-4 airplane are shown in figure 23, as obtained from reference 2. Measured values are considerably lower than the calculated values and, for the highest altitude test, became zero at a Mach number of about 0.85. At a Mach number of 0.88, a sustained oscillation of small amplitude was obtained in the flight test which yielded a large positive value of $C_{m_q} + C_{m_{\dot{\alpha}}}$. Because this oscillation was of small amplitude, the value shown can be considered valid only for small-amplitude motions. The measured values showed an effect of altitude, which, as stated in reference 2, may indicate that aeroelasticity has a large effect on the damping in this case.

Airplane 3.- The results for the F-86 airplane in figure 24 were taken from reference 1. The sharp drop in the experimental curve at $M = 0.92$ was confirmed by a number of separate test points and corresponds to a similar irregular variation in the static stability parameter C_{m_α}. Definite reason for these fairly sharp changes was not established in the preliminary investigation of reference 1 but they are similar to those for other swept-wing configurations (models 3, 4, 9, and 15).

The estimated damping contributed by the tail and the tail plus wing are shown in figure 24. Tail contributions were calculated from lift-curve slopes and downwash values obtained from transonic bump tests of 35° swept wings. Although reference 34 contains tail effectiveness data ($\partial C_m/\partial i_t$) these were not used in calculating the damping because the values measured were about 25 percent lower than would be obtained by using the lift-curve slopes of an isolated 35° swept-tail surface. This is probably primarily caused by the fact that the inboard portion of the adjustable stabilizer (approximately 10 percent of the span) does not move. The lift contributed by the entire surface, however, is effective in producing damping. The damping contributed by the wing was appreciable at subsonic speeds for this configuration and a comparison of the calculated and experimental data indicates that the damping due to the wing is approximately zero at Mach numbers near 1.0.

Airplane 4.- The damping data shown in figure 25 for the D-558-II airplane were taken from reference 35. The calculated damping agrees fairly well with the experimental data at Mach numbers up to about 0.75, but as the Mach number increases, the experimental data show, first, a more rapid increase, and, then, a more rapid decrease than the calculated values. The more rapid decrease may be attributed, at least partially, to a probable dynamically unstable contribution of the wing as shown by model 3 and airplane 2.

GENERALIZATION OF RESULTS

A generalization of results on damping derivatives is limited by the number and types of configurations and the continuity of the experimental flight data available for summary. Some general trends are noted for each type of configuration and a discussion is presented on the computation of damping. The general trends noted are limited for some of the cases by inconclusive evidence.

Tailless Configurations

Four of the five tailless configurations (models 2, 3, and 4, and airplane 2) exhibited either very small negative values or positive values of $C_{m_q} + C_{m_{\dot{\alpha}}}$ in the transonic region. The fifth configuration (model 1), with a 60° triangular wing, showed a fairly smooth variation through the transonic region with no indication of a decrease in damping similar to that encountered on the swept-wing configurations. On model 2 and airplane 2 the positive (unstable) damping coefficients were obtained from small-amplitude sustained oscillations and the evidence indicates that the damping is nonlinear with amplitude, being less at the smaller amplitudes. The data shown for model 1 were obtained from fairly large-amplitude oscillations but other models having the same wing on a slightly different fuselage have been flown with no pitch disturbance applied (unpublished) and no sustained oscillations were encountered.

Examination and comparison of the data for models 3A, 3B, and 4 show that the damping of swept wings is dependent on the flexibility. Also, these data show that similar swept wings exhibit similar variations of damping with Mach number, characterized by a rapid decrease in damping above $M = 0.85$ which would not appear to be a critical Mach number effect. This same decrease in damping is evident for airplane 2.

Wingless Configurations

Data are shown for only one wingless configuration (model 5) and indicate little variation in the damping coefficients with Mach number. It is reasonable to expect that the damping contributed by any lifting surface having a large moment arm from the center of gravity should vary with Mach number in a manner similar to its lift-curve slope if it is not operating in the flow field from a forward surface.

Wing-Plus-Tail Configurations

None of the configurations having tail surfaces exhibited any positive values of $C_{m_q} + C_{m_{\dot{\alpha}}}$ through the Mach number range tested, although several experienced large changes in the transonic region resulting in some fairly small negative damping coefficients. The contribution of an unswept wing to the damping derivatives of the total configuration is usually erratic and may be either positive or negative in the transonic region. In the majority of the cases the damping of the unswept-wing configurations was nonlinear with lift coefficient.

In general the swept-wing configurations having 45° or less sweep also showed erratic changes in damping in the transonic region although

such changes were not as severe as those for the tailless swept-wing configurations because of the smaller contribution of the wing to the total damping. The one 60° swept-wing configuration discussed had a fairly smooth variation with Mach number near M = 1.0. The triangular-wing configurations generally had a somewhat smoother variation with Mach number than those with unswept or swept wings. Modifying or thickening the airfoil sections of the triangular wing (models 11 and 18) seems to result in somewhat less smooth variations in damping with Mach number.

The results for model 17 show that the orientation in roll of the cruciform wings and tails with respect to each other had a significant effect on the damping. It has previously been shown in reference 36 that the tail bending of a configuration similar to model 18 appreciably affected the damping in roll. It is probable that tail flexibility effects also influence the pitch damping.

Canard Configurations

It appears that for the canard configurations shown, the experimental data are less amenable to accurate prediction, probably because of large interference effects and in the case of model 22 by nonlinearities in all the aerodynamic characteristics. Practically no experimental data are available at transonic speeds on the downwash and interference effects applicable to canard configurations.

The contribution to the damping coefficients of the downwash caused by the canard lift increments $C_{L_{\dot{q}}}$ and $C_{L_{\dot{\alpha}}}$ was appreciable for all the canard configurations considered and it appears that this effect should not be neglected for any configuration in which the forward lifting surface is at a large distance (either forward or rearward) of the center of gravity.

Agreement of Calculations and Experiment

It has been generally shown that a computation of the damping contributed by the tail can be made and it will agree reasonably well with the experimental damping. If it is assumed that the downwash lag effect of the wing on the tail is that effect caused by the change in downwash in the finite interval of time required for air to travel from the trailing edge of the mean aerodynamic chord to the tail rather than from the center of gravity to the tail, then the damping due to the tail will exhibit better agreement with experimental data and will be a more conservative estimate.

There exists no suitable means of calculating the wing contribution to damping in the Mach number region from 0.80 to 1.20 and a smoothly faired curve through this region from subsonic to supersonic speeds is of no value except possibly for triangular wings having rounded airfoil sections and which are not in the presence of a wake from a canard surface.

The means of calculating the isolated surface contribution to damping by using references 5 to 8, 11, and 12 generally give values that are nonconservative but are in reasonable agreement with experiment if used within the limitations imposed by the theory.

It should be noted that for computation of wing damping at supersonic speeds, acceptable results are obtained only if $-C_{m_q}$ and $C_{m_{\dot{\alpha}}}$ are both used since the effects are generally in opposite directions. Computations of the damping derivatives for swept wings at lower supersonic Mach numbers by use of references 7 and 8 are extremely limited by the theory.

CONCLUSIONS

From a study of the pitch-damping derivatives measured in flight on about 33 models and full-scale airplanes of widely differing configuration and geometric characteristics, the following general conclusions are offered.

1. No suitable means exist for calculating the wing damping in the transonic region and a smoothly faired line between the subsonic and supersonic values will, in most cases, not conform to the experimental data and will probably give an unconservative result.

2. The damping contribution of unswept and swept wings of 45° or less sweep is erratic in the transonic region and may be either positive or negative, leading to possible dynamic instability for tailless configurations.

3. Configurations with triangular and swept wings having approximately 60° sweep of the leading edge and rounded airfoil sections exhibit fairly smooth variations of damping in the transonic region.

4. Calculations of the damping for configurations that have a horizontal tail surface appear to give the best agreement with the experimental data if the distance from the trailing edge of the mean aerodynamic chord of the wing to the tail is used for computing the downwash lag.

5. Damping moments resulting from the downwash on a rear lifting surface caused by the lift increments on a forward surface proportional to the pitching velocity and the rate of change of angle of attack may be appreciable if the forward surface is at a large distance from the center of gravity, as on a canard configuration.

It is believed that no detailed conclusions are warranted because of the unsystematic nature of the data and the effects of relatively unknown factors such as experimental accuracy, nonlinearities with lift coefficient and oscillation amplitude, and the effects of oscillation frequency.

Langley Aeronautical Laboratory,
National Advisory Committee for Aeronautics,
Langley Field, Va.

REFERENCES

1. Triplett, William C., and Van Dyke, Rudolph D., Jr.: Preliminary Flight Investigation of the Dynamic Longitudinal-Stability Characteristics of a 35° Swept-Wing Airplane. NACA RM A50J09a, 1950.

2. Sadoff, Melvin, Ankenbruck, Herman O., and O'Hare, William: Stability and Control Measurements Obtained During USAF-NACA Cooperative Flight-Test Program on the X-4 Airplane (USAF No. 46-677). NACA RM A51H09, 1951.

3. Gillis, Clarence L., Peck, Robert F., and Vitale, A. James: Preliminary Results From a Free-Flight Investigation at Transonic and Supersonic Speeds of the Longitudinal Stability and Control Characteristics of an Airplane Configuration With a Thin Straight Wing of Aspect Ratio 3. NACA RM L9K25a, 1950.

4. Jones, B. Melvill: Dynamics of the Airplane. Symmetric or Pitching Moments. Vol. V of Aerodynamic Theory, div. N, ch. II, secs. 37-44, W. F. Durand, ed., Julius Springer (Berlin), 1935, pp. 48-54.

5. Harmon, Sidney M.: Stability Derivatives at Supersonic Speeds of Thin Rectangular Wings With Diagonals Ahead of Tip Mach Lines. NACA Rep. 925, 1949. (Supersedes NACA TN 1706.)

6. Ribner, Herbert S., and Malvestuto, Frank S., Jr.: Stability Derivatives of Triangular Wings at Supersonic Speeds. NACA Rep. 908, 1948. (Supersedes NACA TN 1572.)

7. Malvestuto, Frank S., Jr., and Hoover, Dorothy M.: Supersonic Lift and Pitching Moment of Thin Sweptback Tapered Wings Produced by Constant Vertical Acceleration. Subsonic Leading Edges and Supersonic Trailing Edges. NACA TN 2315, 1951.

8. Malvestuto, Frank S., Jr., and Hoover, Dorothy M.: Lift and Pitching Derivatives of Thin Sweptback Tapered Wings With Streamwise Tips and Subsonic Leading Edges at Supersonic Speeds. NACA TN 2294, 1951.

9. Tobak, Murray, Reese, David E., Jr., and Beam, Benjamin H.: Experimental Damping in Pitch of 45° Triangular Wings. NACA RM A50J26, 1950.

10. D'Auitolo, Charles T., and Parker, Robert N.: Preliminary Investigation of the Low-Amplitude Damping in Pitch of Tailless Delta- and Swept-Wing Configurations at Mach Numbers From 0.7 to 1.35. NACA RM L52G09, 1952.

11. Toll, Thomas A., and Queijo, M. J.: Approximate Relations and Charts for Low-Speed Stability Derivatives of Swept Wings. NACA TN 1581, 1948.

12. Fisher, Lewis R.: Approximate Corrections for the Effects of Compressibility on the Subsonic Stability Derivatives of Swept Wings. NACA TN 1854, 1949.

13. Jones, Robert T., and Fehlner, Leo F.: Transient Effects of the Wing Wake on the Horizontal Tail. NACA TN 771, 1940.

14. Ribner, Herbert S.: Time-Dependent Downwash at the Tail and the Pitching Moment Due to Normal Acceleration at Supersonic Speeds. NACA TN 2042, 1950.

15. Mitchell, Jesse L.: The Static and Dynamic Longitudinal Stability Characteristics of Some Supersonic Aircraft Configurations. NACA RM L52A10a, 1952.

16. Beam, Benjamin H.: The Effects of Oscillation Amplitude and Frequency on the Experimental Damping in Pitch of a Triangular Wing Having an Aspect Ratio of 4. NACA RM A52G07, 1952.

17. Mitcham, Grady L., Crabill, Norman L., and Stevens, Joseph E.: Flight Determination of the Drag and Longitudinal Stability and Control Characteristics of a Rocket-Powered Model of a 60° Delta-Wing Airplane From Mach Numbers of 0.75 to 1.70. NACA RM L51I04, 1951.

18. Henderson, Arthur, Jr.: Pitching-Moment Derivatives C_{m_q} and $C_{m_{\dot{\alpha}}}$ at Supersonic Speeds for a Slender-Delta-Wing and Slender-Body Combination and Approximate Solutions for Broad-Delta-Wing and Slender-Body Combinations. NACA TN 2553, 1951.

19. Smith, C. B., and Beane, Beverly J.: Damping in Pitch of Bodies of Revolution at Supersonic Speeds. Preprint No. 311, Inst. Aero. Sci., Feb. 1951.

20. Gillis, Clarence L., and Vitale, A. James: Wing-On and Wing-Off Longitudinal Characteristics of an Airplane Configuration Having a Thin Unswept Tapered Wing of Aspect Ratio 3, As Obtained From Rocket-Propelled Models at Mach Numbers From 0.8 to 1.4. NACA RM L50K16, 1951.

21. Parks, James H.: Longitudinal Aerodynamic Characteristics of a Model Airplane Configuration Equipped With a Scaled X-1 Airplane Wing. NACA RM L51L10a, 1952.

22. Mattson, Axel T., and Loving, Donald L.: Force, Static Longitudinal Stability, and Control Characteristics of a $\frac{1}{16}$ -Scale Model of the Bell XS-1 Transonic Research Airplane at High Mach Numbers. NACA RM L8A12, 1948.

23. Vitale, A. James, McFall, John C., Jr., and Morrow, John D.: Longitudinal Stability and Drag Characteristics at Mach Numbers From 0.75 to 1.5 of an Airplane Configuration Having a 60° Swept Wing of Aspect Ratio 2.24 As Obtained From Rocket-Propelled Models. NACA RM L51K06, 1952.

24. Chapman, Rowe, Jr., and Morrow, John D.: Longitudinal Stability and Drag Characteristics at Mach Numbers From 0.70 to 1.37 of Rocket-Propelled Models Having a Modified Triangular Wing. NACA RM L52A31, 1952.

25. Peck, Robert F., and Mitchell, Jesse L.: Rocket-Model Investigation of Longitudinal Stability and Drag Characteristics of an Airplane Configuration Having a 60° Delta Wing and a High Unswept Horizontal Tail. NACA RM L52K04a, 1952.

26. Parks, James H., and Kehlet, Alan B.: Longitudinal Stability, Trim, and Drag Characteristics of a Rocket-Propelled Model of an Airplane Configuration Having a 45° Sweptback Wing and an Unswept Horizontal Tail. NACA RM L52F05, 1952.

27. D'Aiutolo, Charles T., and Mason, Homer P.: Preliminary Results of the Flight Investigation Between Mach Numbers of 0.80 and 1.36 of a Rocket-Powered Model of a Supersonic Airplane Configuration Having a Tapered Wing With Circular-Arc Sections and 40° Sweepback. NACA RM L50H29a, 1950.

28. Mitcham, Grady L., and Blanchard, Willard S., Jr.: Summary of the Aerodynamic Characteristics and Flying Qualities Obtained From Flights of Rocket-Propelled Models of an Airplane Configuration Incorporating a Sweptback Inversely Tapered Wing at Transonic and Low-Supersonic Speeds. NACA RM L50G18a, 1950.

29. Hall, James R.: Free-Flight Investigation of Longitudinal Stability and Control of a Rocket-Propelled Missile Model Having Cruciform, Triangular, Inline Wings and Tails. NACA RM L51J17, 1952.

30. Edwards, Samuel Sherman: Experimental and Theoretical Study of Factors Influencing the Longitudinal Stability of an Air-to-Air Missile at a Mach Number of 1.4. NACA RM A51J19, 1952.

31. Moul, Martin T., and Wineman, Andrew R.: Longitudinal Stability and Control Characteristics From a Flight Investigation of a Cruciform Canard Missile Configuration Having an Exposed Wing-Canard Area Ratio of 16:1. NACA RM L52D24a, 1952.

32. Brown, Clarence A., Jr., and Lundstrom, Reginald R.: Flight Investigation From Mach Number 0.8 to Mach Number 2.0 To Determine Some Effects of Wing-To-Tail Distance on the Longitudinal Stability and Control Characteristics of a 60° Delta-Wing - Canard Missile. NACA RM L52C26, 1952.

33. Angle, Ellwyn E., and Holleman, Euclid C.: Determination of Longitudinal Stability of the Bell X-1 Airplane From Transient Responses at Mach Numbers up to 1.12 at Lift Coefficients of 0.3 and 0.6. NACA RM L50I06a, 1950.

34. Morrill, Charles P., Jr., and Boddy, Lee E.: High-Speed Stability and Control Characteristics of a Fighter Airplane Model With a Swept-Back Wing and Tail. NACA RM A7K28, 1948.

35. Holleman, Euclid C.: Longitudinal Frequency-Response and Stability Characteristics of the Douglas D-558-II Airplane As Determined From Transient Response to a Mach Number of 0.96. NACA RM L52E02, 1952.

36. Hopko, Russell N.: A Flight Investigation of the Damping in Roll and Rolling Effectiveness Including Aeroelastic Effects of Rocket-Propelled Missile Models Having Cruciform, Triangular, Interdigitated Wings and Tails. NACA RM L51D16, 1951.

TABLE I

AIRFOIL SECTION CHARACTERISTICS

(Measured parallel to free stream unless otherwise stated)

Model	Type section	Number or percent thickness at root	Number or percent thickness at tip	Remarks
1	NACA	$65_{(06)}$A006.5	$65_{(06)}$A006.5	
2	NACA	0007-63/30-9.5° mod.	0007-63/30-9.5° mod.	
3	NACA	65A009	65A009	
4	Round nose	6	6	
5	Hexagonal	4.5	4.5	
6	Hexagonal	4.5	4.5	
7	NACA	$65_{(06)}$A004.5	$65_{(06)}$A004.5	
8	NACA	65-108	65-108	
9	NACA	65A006	65A006	
10	NACA	64A011	64A008	Normal to 0.3266c
11	NACA	0006, mod. to 3.5	0006	
12	NACA	$65_{(06)}$A003	$65_{(06)}$A003	
13	Hexagonal	4.5	4.5	Radii at break lines
14	NACA	65A006	65A006	
15	Circular arc, symmetrical	5	5	Normal to 0.25c
16	Round nose	7.56	7.56	
17	NACA	65A009	65A009	
18	Double wedge	4	4	
19	NACA	$66_{(06)}$-002.84	66-006	
20	Hexagonal	3.1	9.3	
21	Hexagonal	3.1	9.3	
22	Double wedge	5.0	5.0	

Airplane	Type section	Number or percent thickness at root	Number or percent thickness at tip	Remarks
1	NACA	65-108	65-108	
2	NACA	0010-64	0010-64	
3	NACA	0012-64 mod.	0011-64 mod.	Normal to 0.25c
4	NACA	63-010	63_1-012	Normal to 0.30c

TABLE II

REDUCED-FREQUENCY RANGE

FOR DATA PRESENTED

Model	Range of $\omega c/2V$	
1	0.0212	0.0258
2	.0287	.0455
3	.0186	.0217
4	.0118	.0126
5	.0046	.0053
6	.0119	.0135
7	.0081	.0108
8	.0050	.0072
9	.0081	.0097
10	.0122	.0129
11	.0161	.0169
12	.0165	.0178
13	.0084	.0156
14	.0168	.0207
15	.0164	.0241
16	.0151	.0273
17	.0069	.0134
18	.0089	.0106
19	.0209	.0295
20	.0103	.0125
21	.0058	.0086
22	.0081	.0100

Airplane	Range of $\omega c/2V$	
1	------	------
2	0.0449	0.0539
3	.0155	.0310
4	.0117	.0162

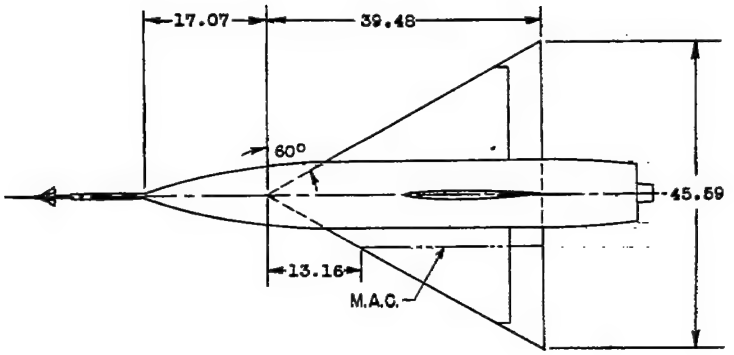

Center-of-gravity location

Model A	20 percent M.A.C.
Model B	25 percent M.A.C.

Wing

A	2.31
S, sq ft	6.25
M.A.C., in.	26.28

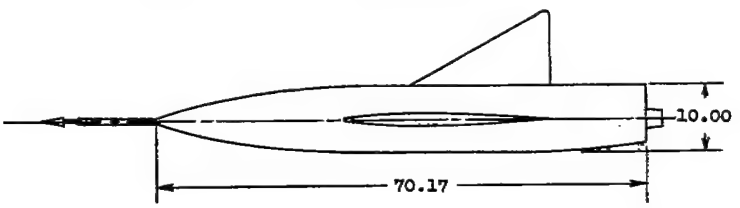

All dimensions are in inches.

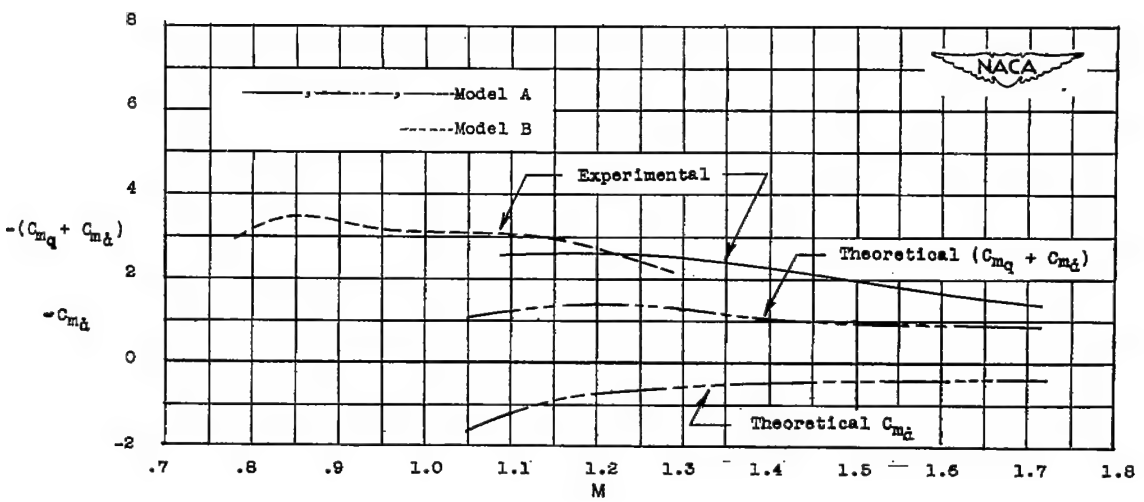

Figure 1.- Geometric characteristics and damping coefficients for a 60° triangular wing aircraft configuration (model 1).

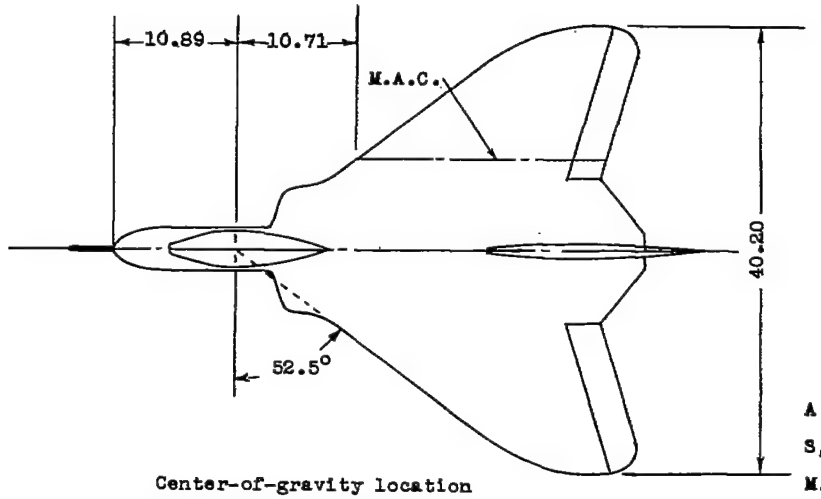

Wing	
A	2.01
S, sq ft	5.57
M.A.C., in.	21.90

Center-of-gravity location

Model A 16.7 percent M.A.C.

Model B 9.9 percent M.A.C.

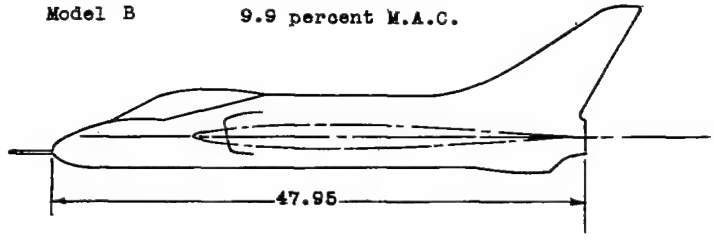

All dimensions are in inches.

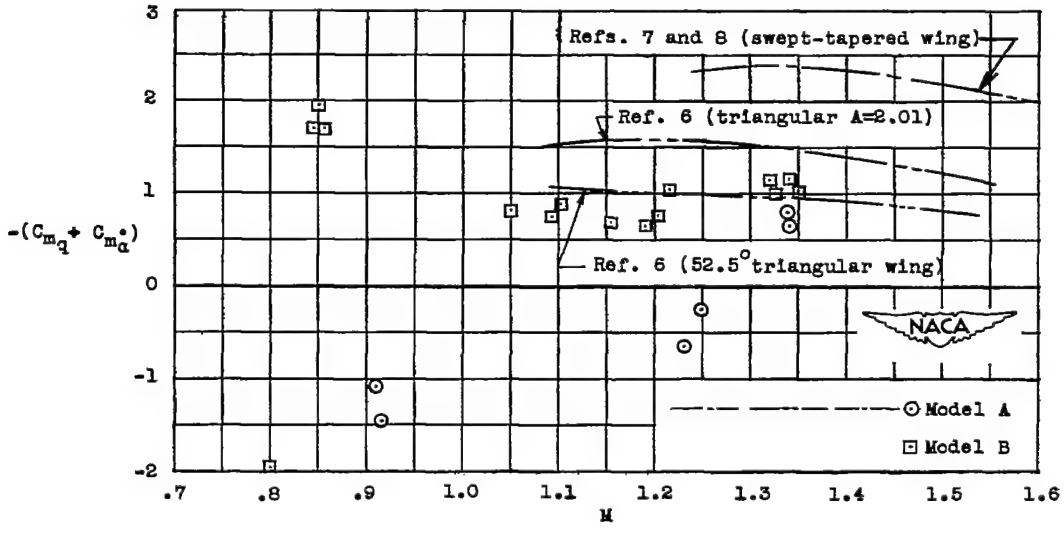

Figure 2.- Geometric characteristics and damping coefficients for a tailless aircraft configuration (model 2).

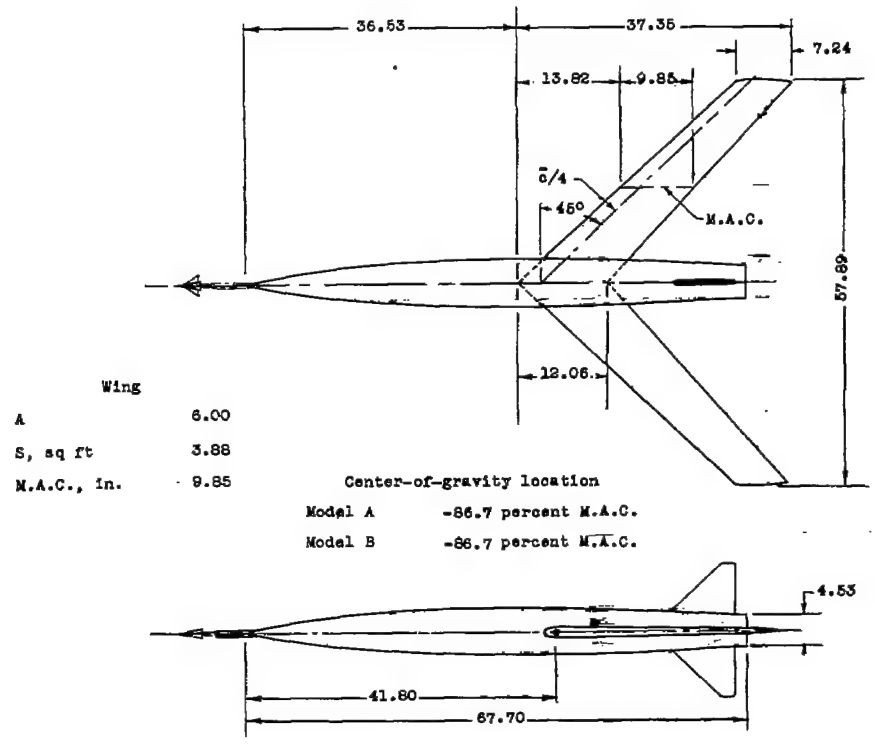

All dimensions are in inches.

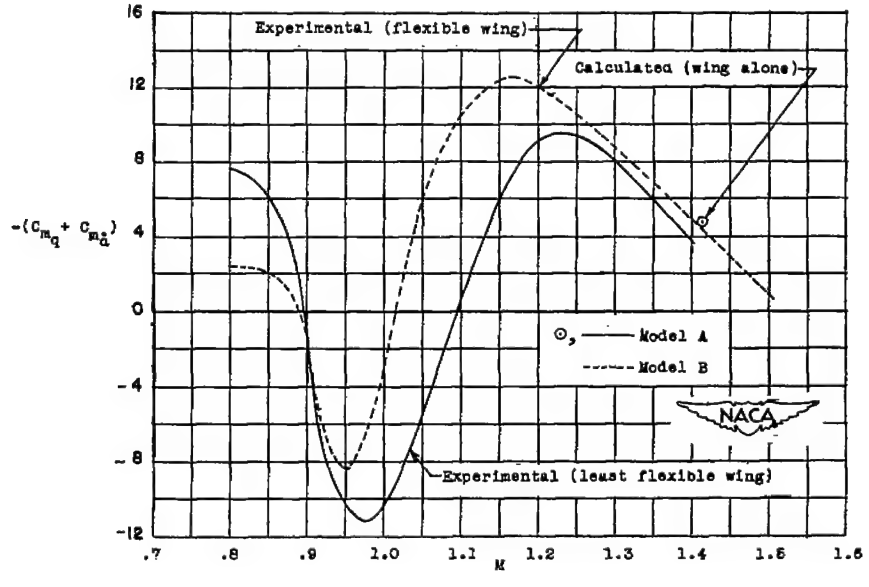

Figure 3.- Geometric characteristics and damping coefficients for a 45° sweptback wing and body configuration (model 3).

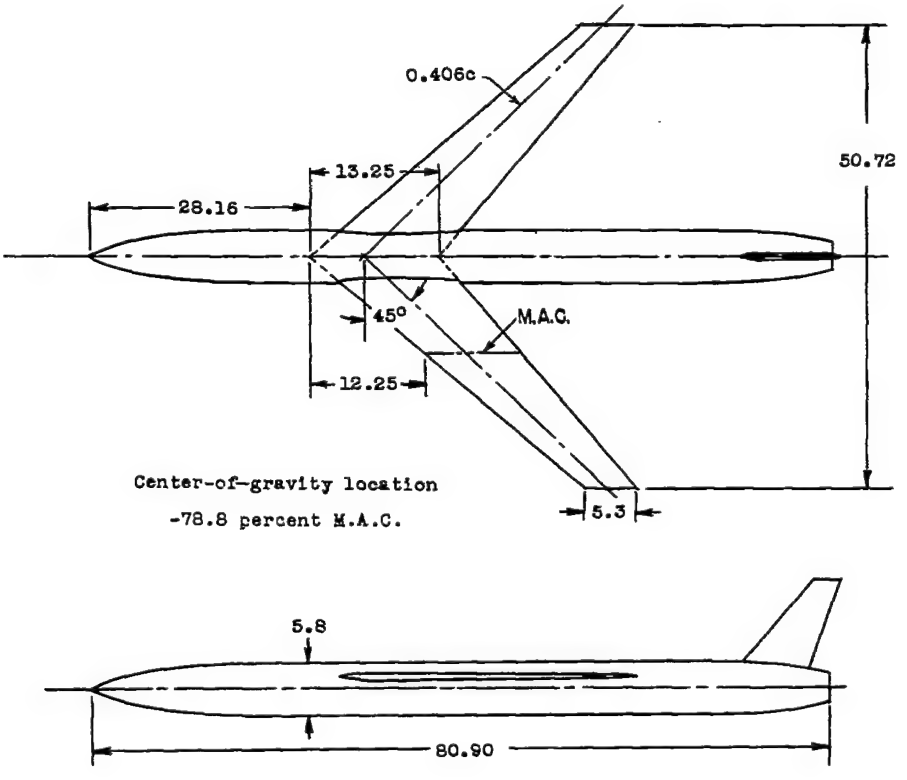

Wing	
A	5.5
S, sq ft	3.27
M.A.C., in.	9.84

All dimensions are in inches.

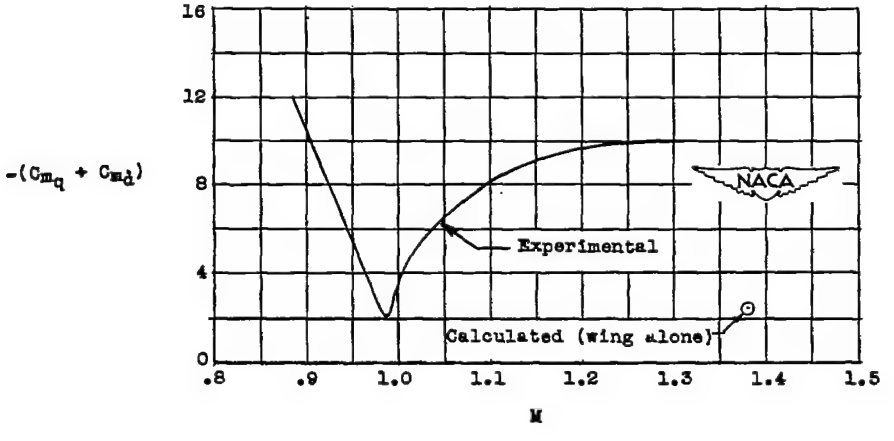

Figure 4.- Geometric characteristics and damping coefficients for a 45° sweptback wing missile configuration (model 4).

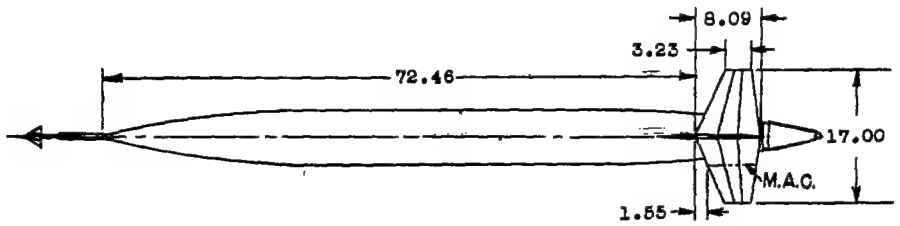

Center-of-gravity location

52.8 percent body length

Horizontal Tail	
A	3.00
S, sq ft	.67
M.A.C., in.	6.01

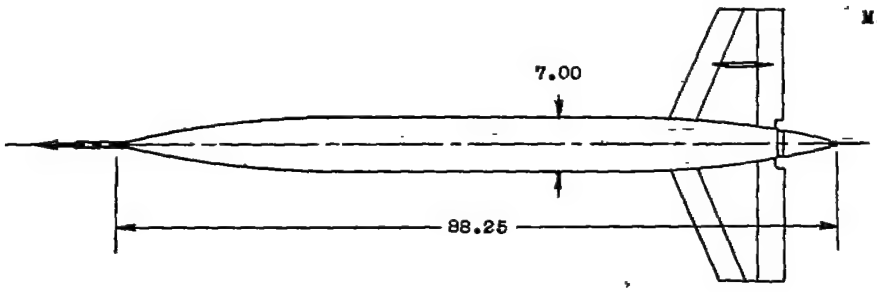

All dimensions are in inches.

Note: Coefficients are based on wing area and wing chord of model 6.

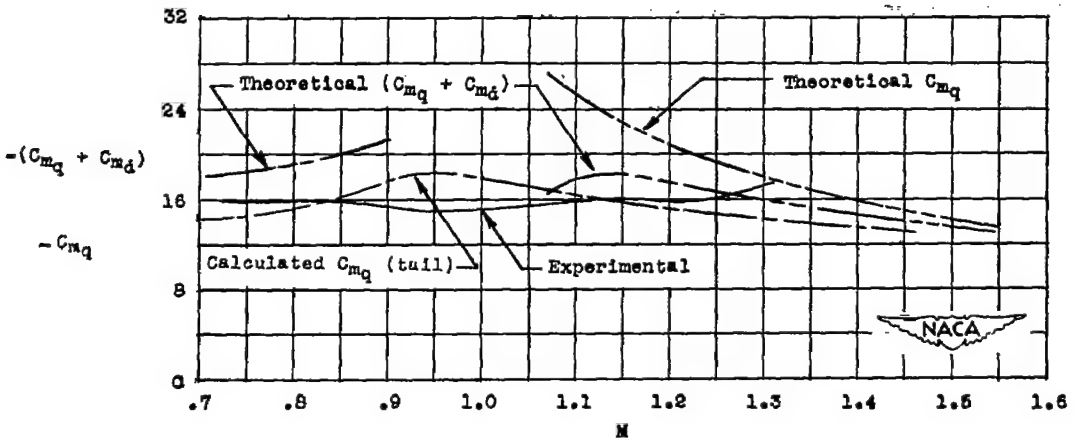

Figure 5.- Geometric characteristics and damping coefficients for a wingless body and horizontal tail combination (model 5).

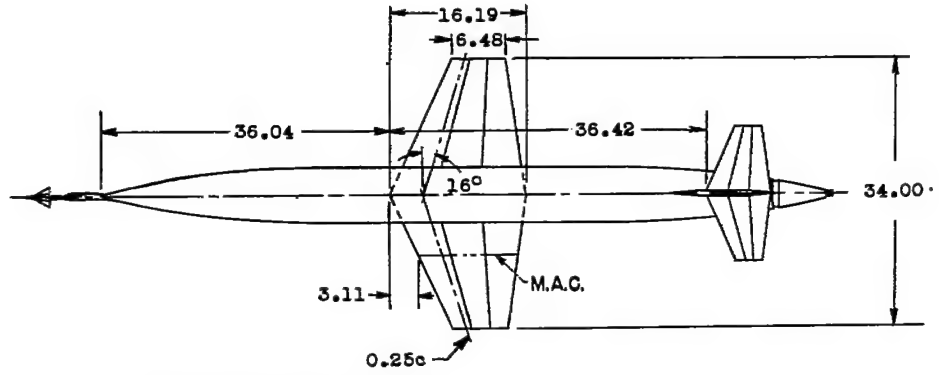

Center-of-gravity location

Model A 12.4 percent M.A.C.

Model B 12.4 percent M.A.C.

Wing	
A	3.00
S, sq ft	2.68
M.A.C., in.	12.03

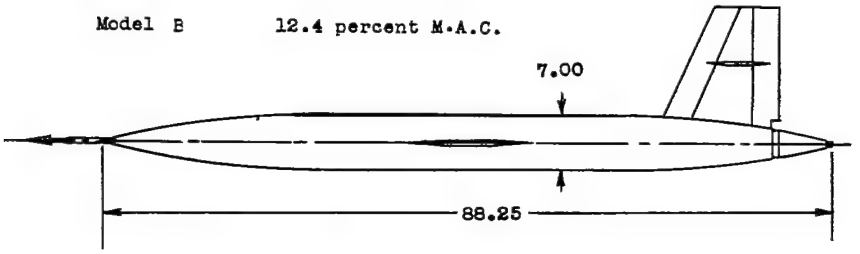

Horizontal Tail

Same as model 5

All dimensions are in inches.

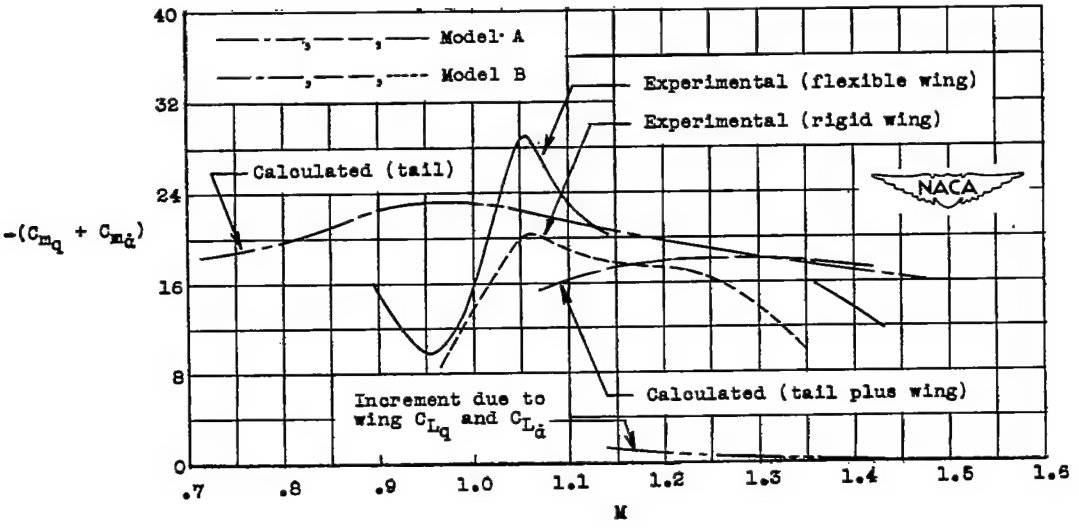

Figure 6.- Geometric characteristics and damping coefficients for an aircraft configuration having an unswept tapered wing with a hexagonal airfoil section (model 6).

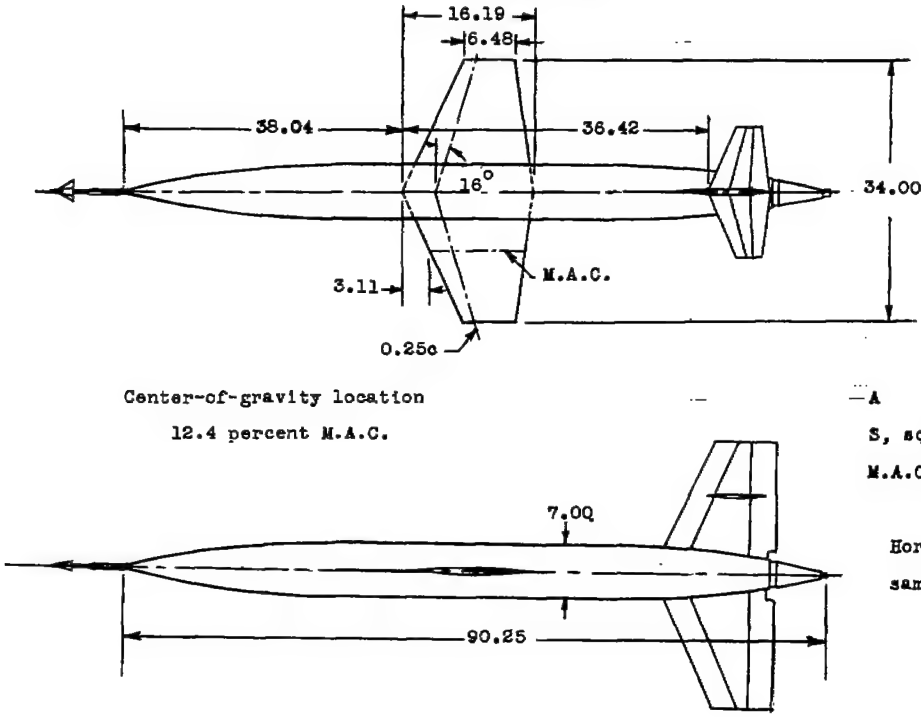

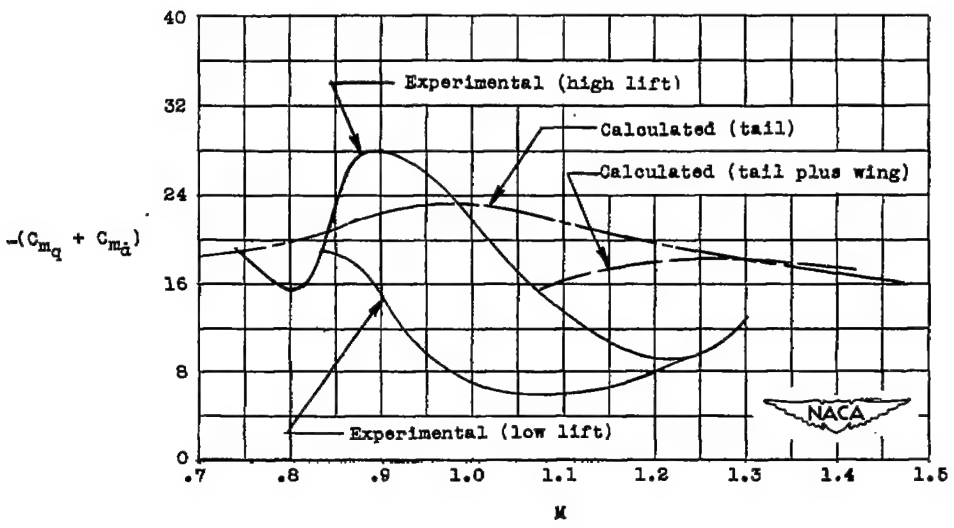

Figure 7.- Geometric characteristics and damping coefficients for an aircraft configuration having an unswept wing with an NACA $65_{(06)}A004.5$ airfoil section (model 7).

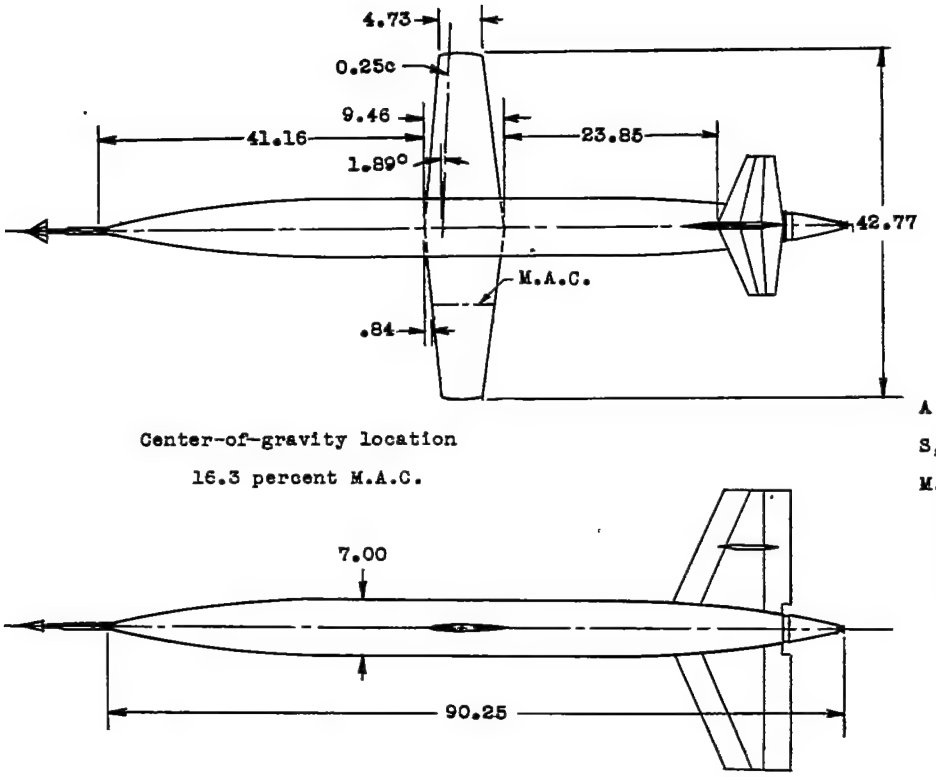

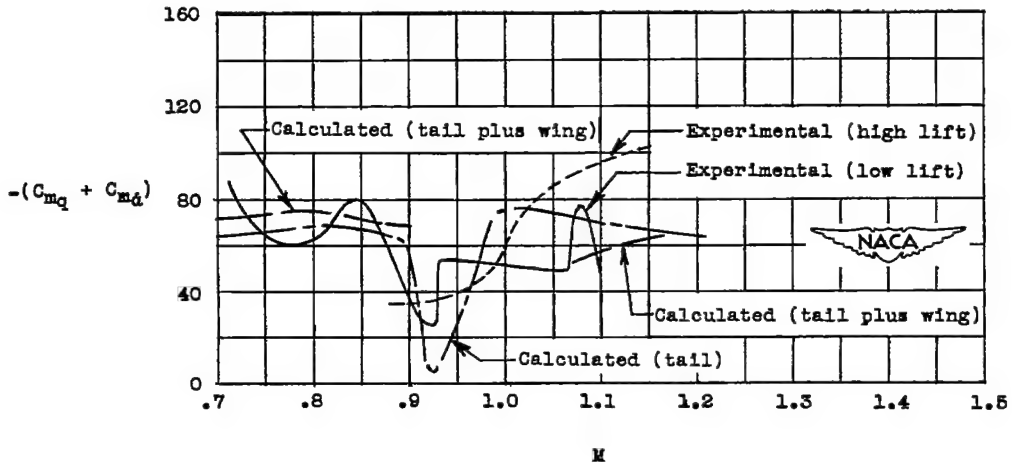

Figure 8.- Geometric characteristics and damping coefficients for an aircraft configuration having the X-1 wing (model 8).

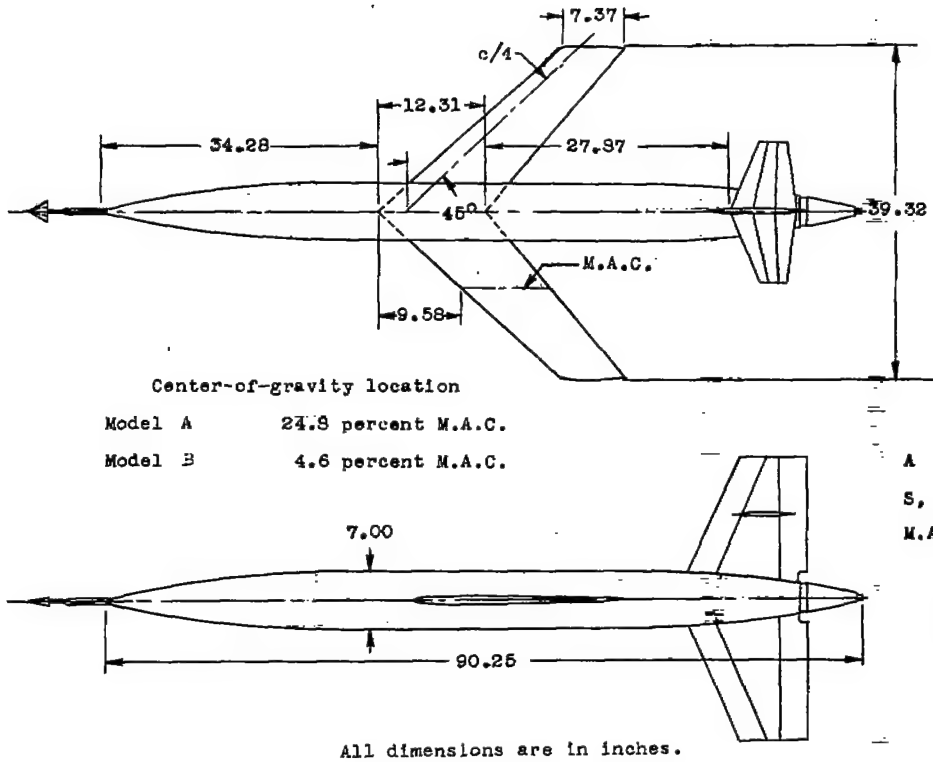

Center-of-gravity location

Model A 24.8 percent M.A.C.

Model B 4.6 percent M.A.C.

Wing	
A	4.00
S, sq ft	2.69
M.A.C., in.	10.05

Horizontal Tail

Same as model 5

All dimensions are in inches.

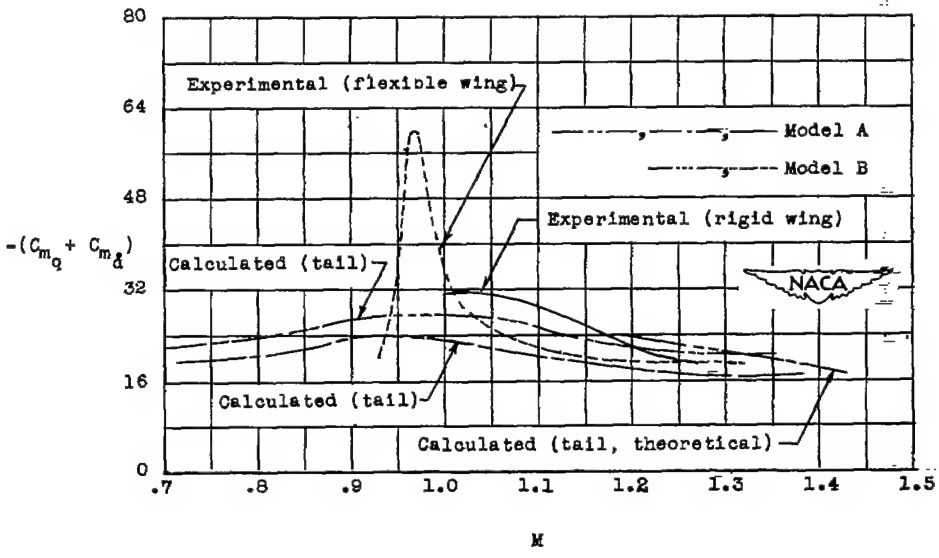

Figure 9.- Geometric characteristics and damping coefficients for an aircraft configuration having a 45° sweptback wing (model 9).

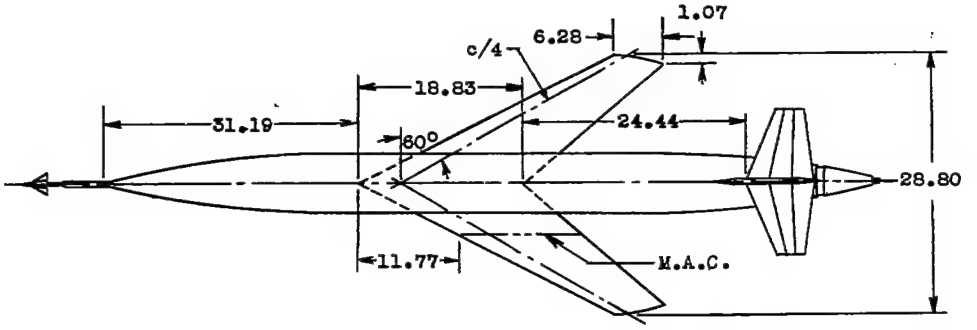

Center-of-gravity location
-4 percent M.A.C.

Wing	
A	2.24
S, sq ft	2.58
M.A.C., in.	14.10

Horizontal Tail
Same as model 5

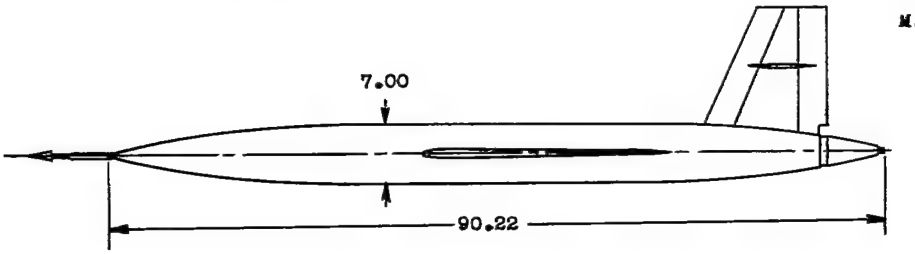

All dimensions are in inches.

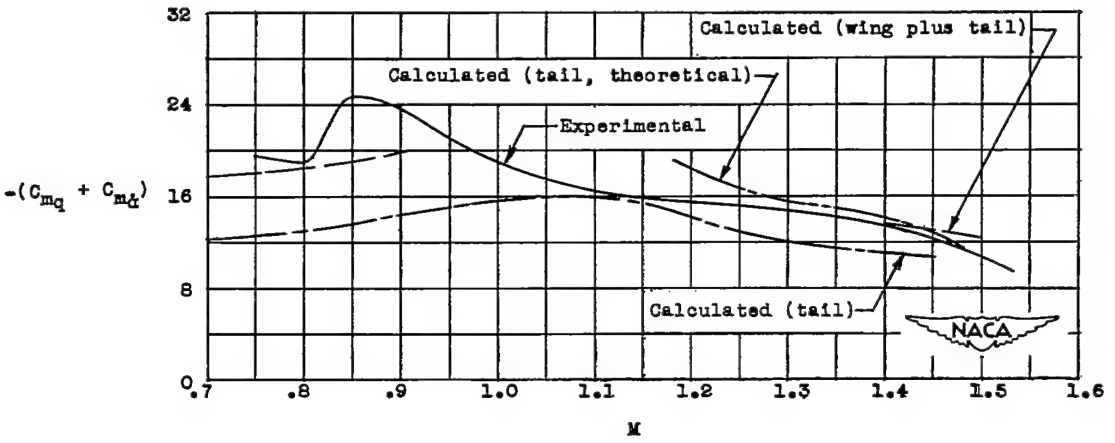

Figure 10.- Geometric characteristics and damping coefficients for an aircraft configuration having a 60° sweptback wing (model 10).

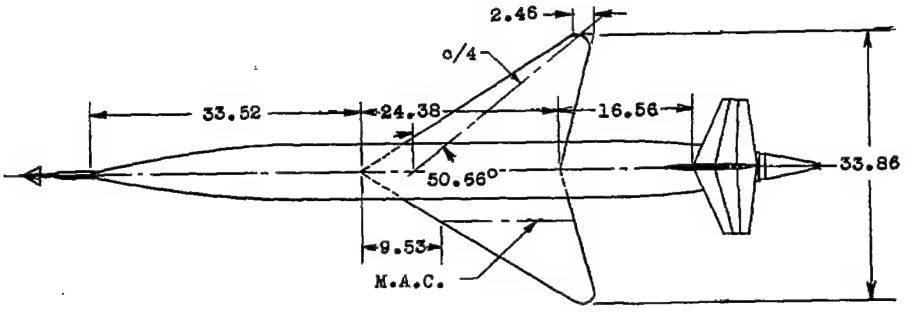

Center-of-gravity location
13.2 percent M.A.C.

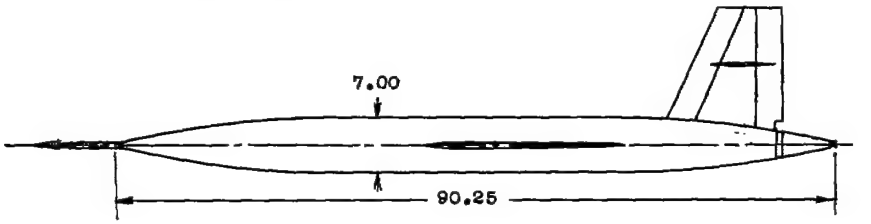

Wing	
A	2.53
S, sq ft	3.14
M.A.C., in.	16.40

Horizontal Tail
Same as model 5

All dimensions are in inches.

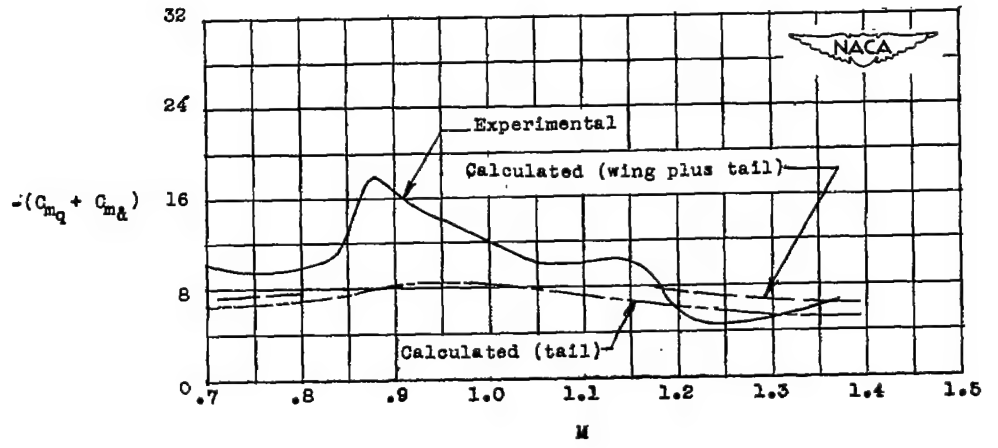

Figure 11.- Geometric characteristics and damping coefficients for an aircraft configuration having a modified triangular wing (model 11).

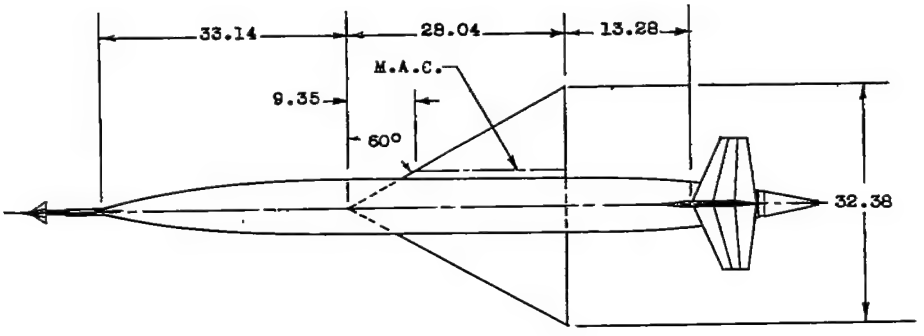

Center-of-gravity location
20.5 percent M.A.C.

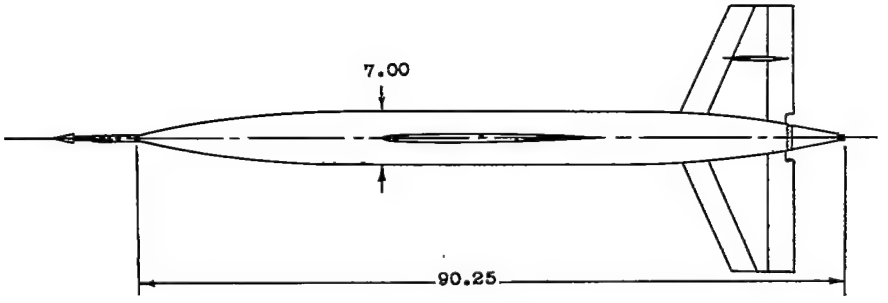

All dimensions are in inches.

Wing	
A	2.31
S, sq ft	3.15
M.A.C., in.	18.70

Horizontal Tail
Same as model 5

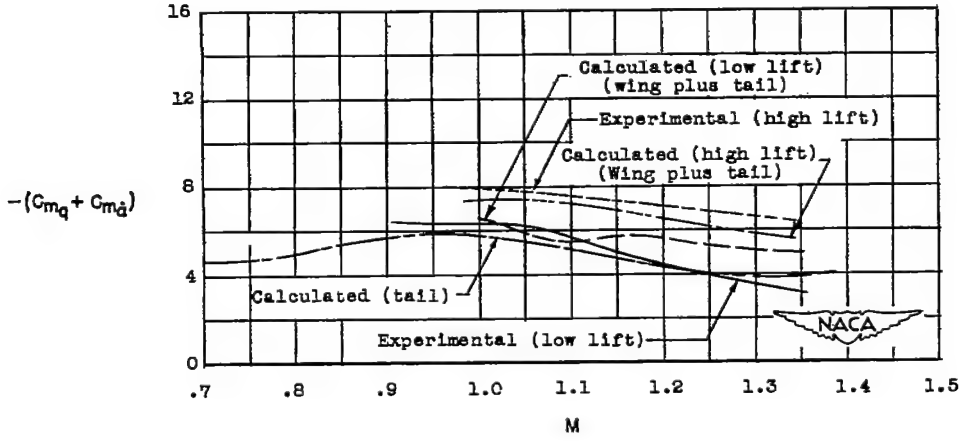

Figure 12.- Geometric characteristics and damping coefficients for an aircraft configuration having a 60° triangular wing (model 12).

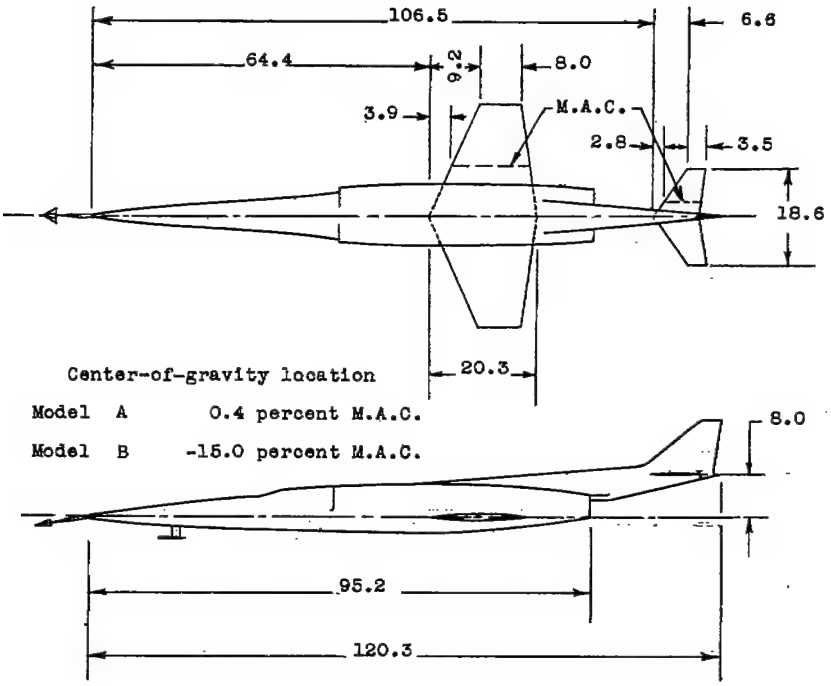

All dimensions are in inches.

Wing	
A	3.0
S, sq ft	4.25
M.A.C., in.	15.1
Span, in.	43.2

Horizontal Tail	
A	3.0
S, sq ft	0.79
M.A.C., in.	6.54

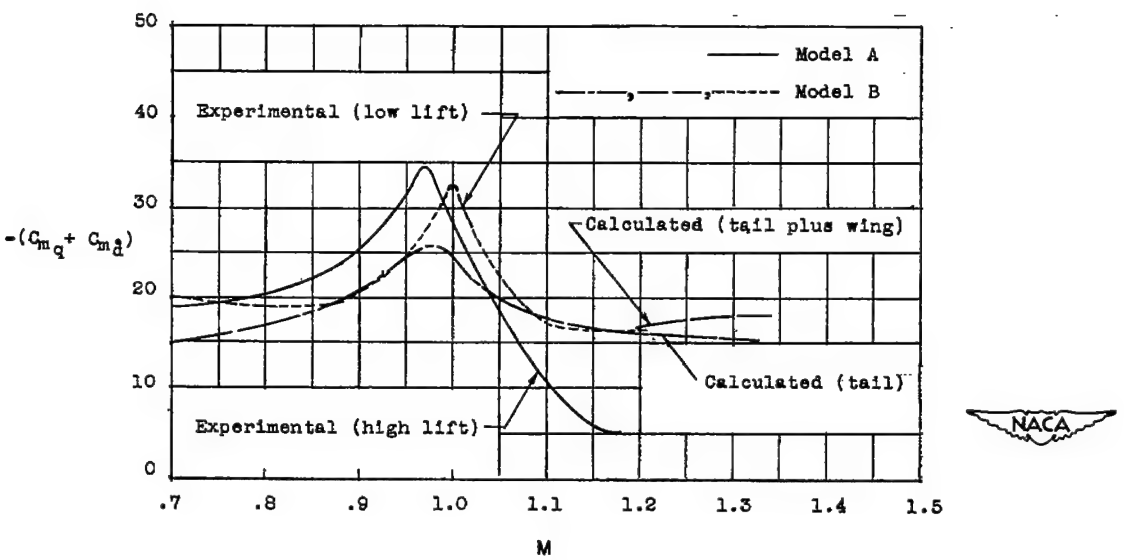

Figure 13.- Geometric characteristics and damping coefficients for a supersonic aircraft configuration (model 13).

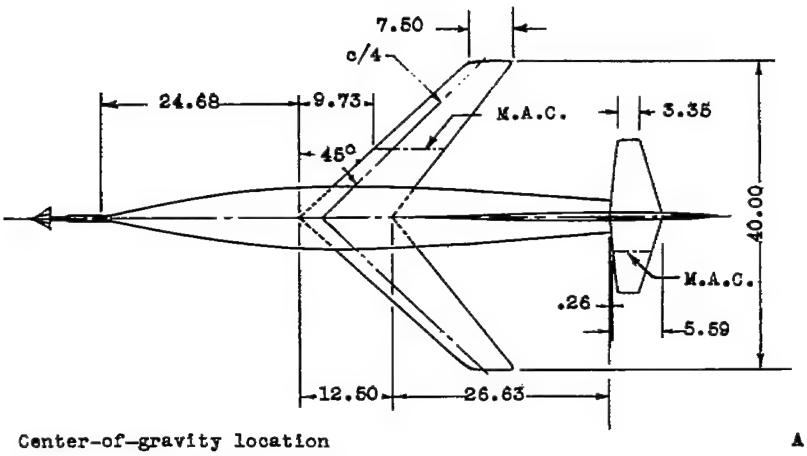

Wing	
A	4.00
S, sq ft	2.77
M.A.C., in.	10.21

Horizontal Tail	
A	4.00
S, sq ft	.55
M.A.C., in.	4.58

All dimensions are in inches.

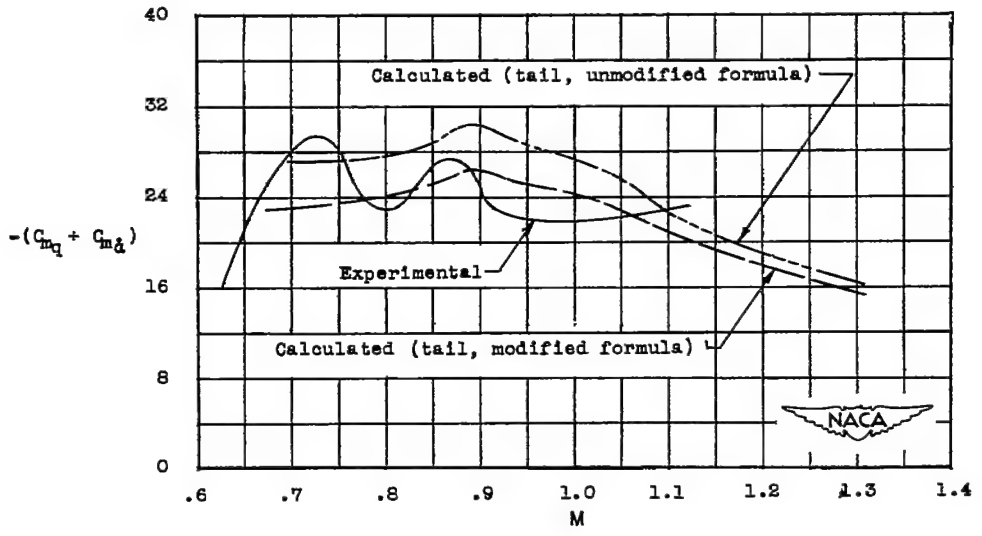

Figure 14.- Geometric characteristics and damping coefficients for an aircraft configuration having a 45° sweptback wing (model 14).

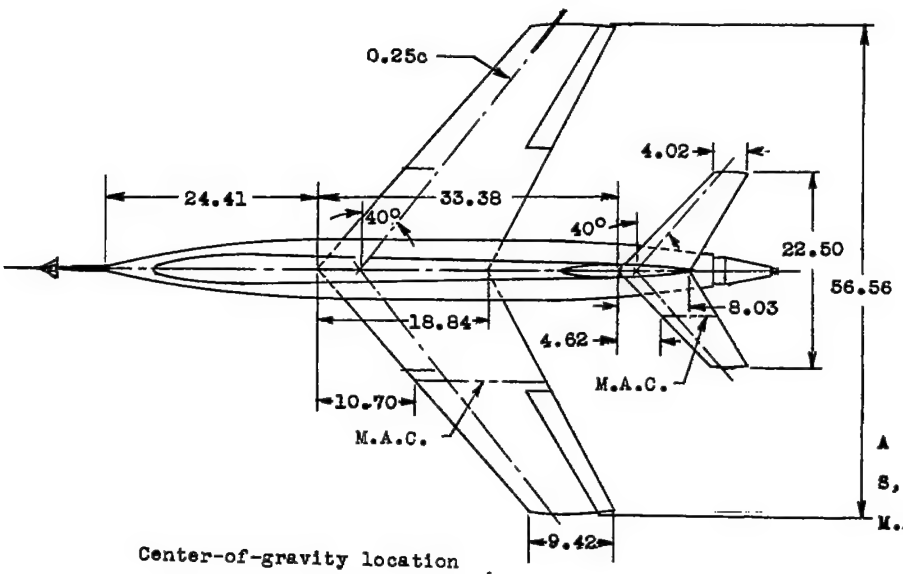

Wing	
A	4.00
S, sq ft	5.56
M.A.C., in.	14.64

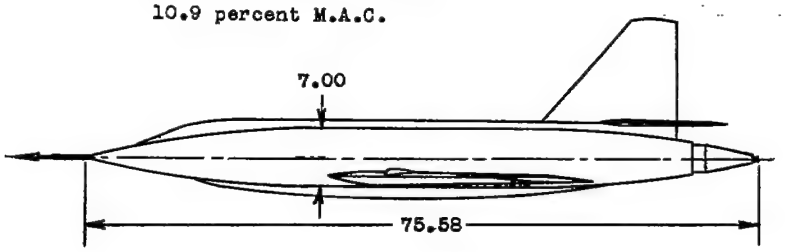

Horizontal Tail	
A	3.72
S, sq ft	.938
M.A.C., in.	6.27

All dimensions are in inches.

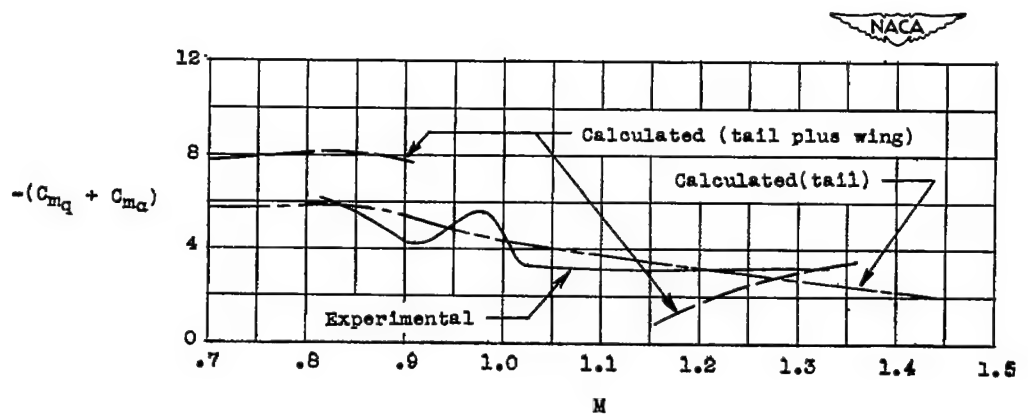

Figure 15.- Geometric characteristics and damping coefficients of an aircraft configuration having a 40° sweptback wing (model 15).

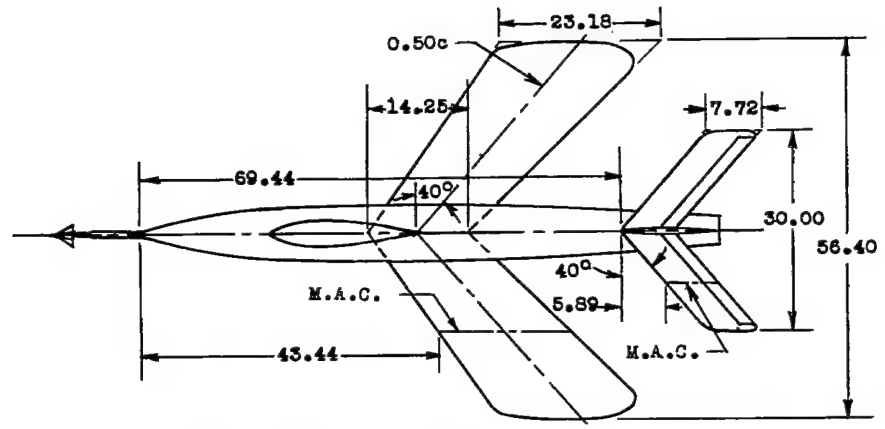

Center-of-gravity location

Model A 12.5 percent M.A.C.

Model B 5.6 percent M.A.C.

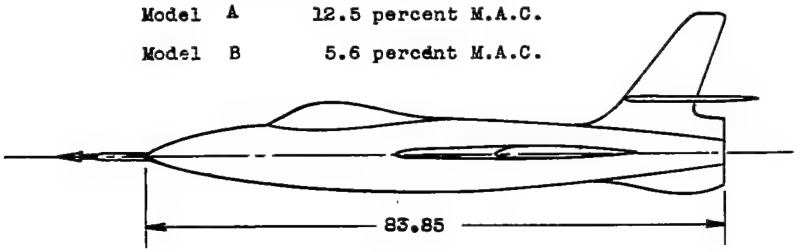

Wing	
A	3.07
S, sq ft	7.20
M.A.C., in.	19.08

Horizontal Tail	
A	3.98
S, sq ft	1.57
M.A.C., in.	7.72

All dimensions are in inches.

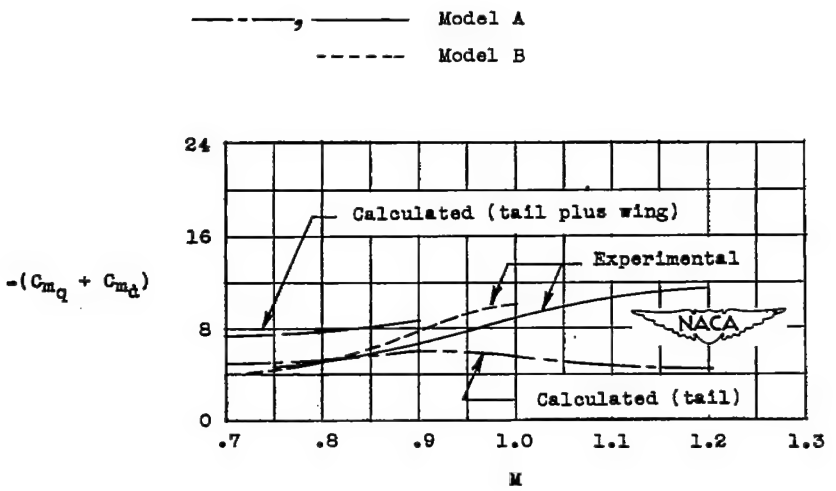

Figure 16.- Geometric characteristics and damping coefficients of an aircraft having a 40° sweptback wing that incorporates inverse taper (model 16).

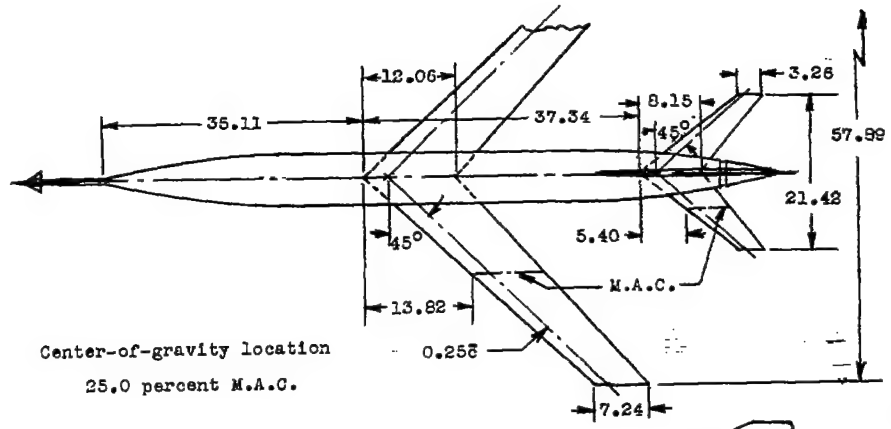

All dimensions are in inches.

Wing	
A	6.00
S, sq ft	3.88
M.A.C., in.	9.85
Horizontal tail	
A	4.00
S, sq ft (in chord plane)	.90
M.A.C., in.	6.05
Dihedral	-20°

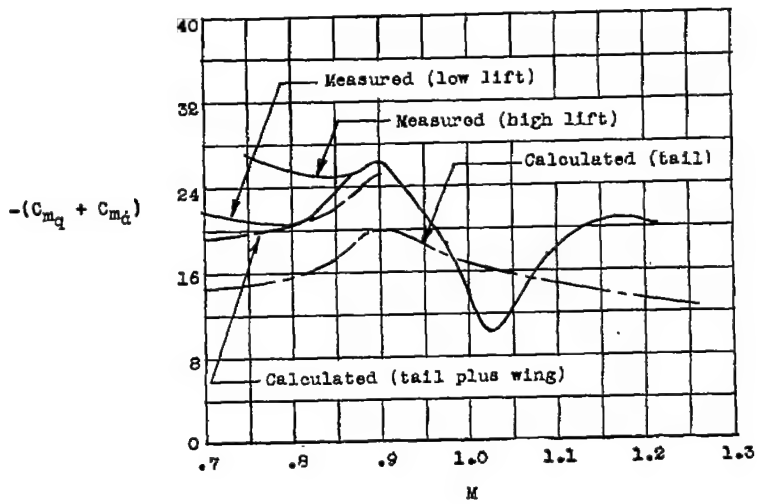

Figure 17.- Geometric characteristics and damping coefficients for an aircraft configuration having a 45° sweptback wing (model 17).

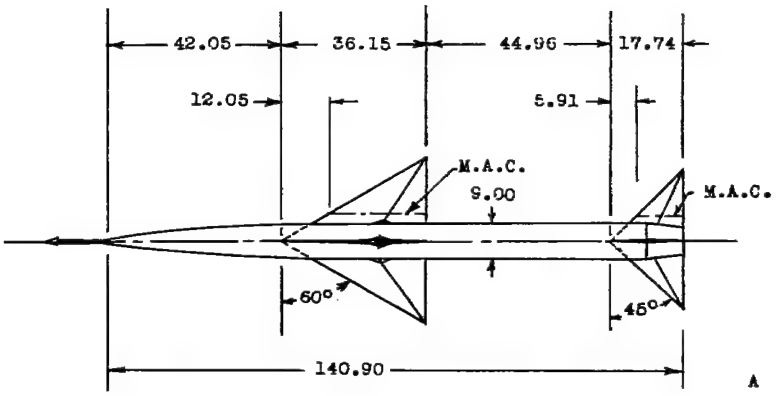

Wing	
A	2.31
S, sq ft	5.23
M.A.C., in.	24.10

Horizontal Tail	
A	4.00
S, sq ft	2.19
M.A.C., in.	11.83

Center-of-gravity location

Model A 50.8 percent M.A.C.

Model B 50.8 percent M.A.C.

All dimensions are in inches.

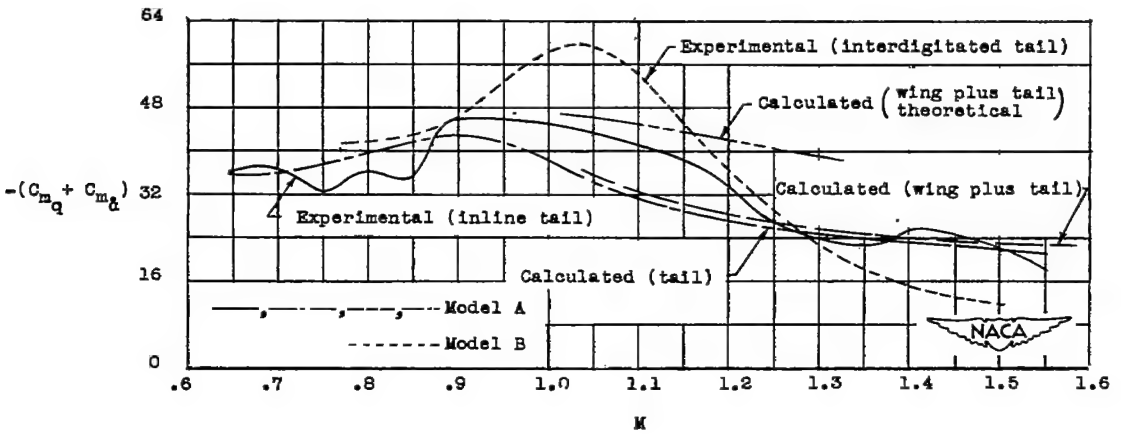

Figure 18.- Geometric characteristics and damping coefficients of a 60° triangular wing missile configuration (model 18).

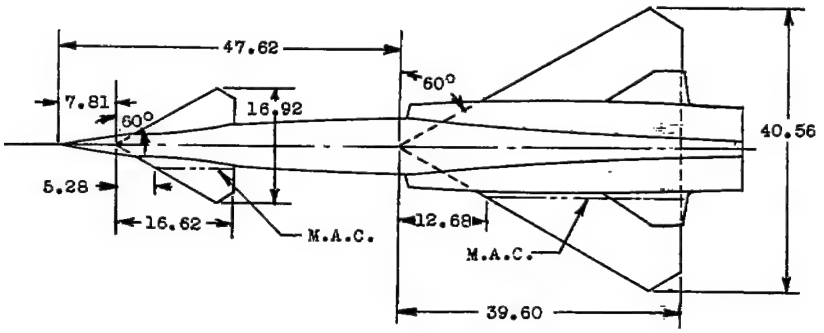

Center-of-gravity location

Station 56.98

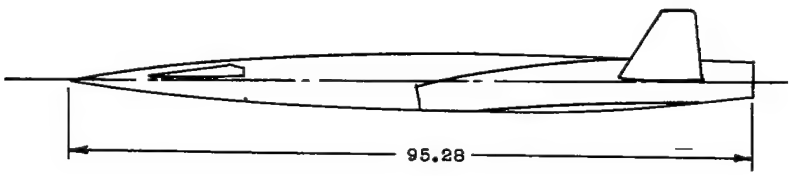

All dimensions are in inches

Wing	
A	1.87
$\bar{S}$, sq ft	6.12
M.A.C., in.	26.94

Canard	
A (in chord plane)	1.87
S, sq ft (in chord plane)	1.08
M.A.C., in.	11.33
Dihedral	15°

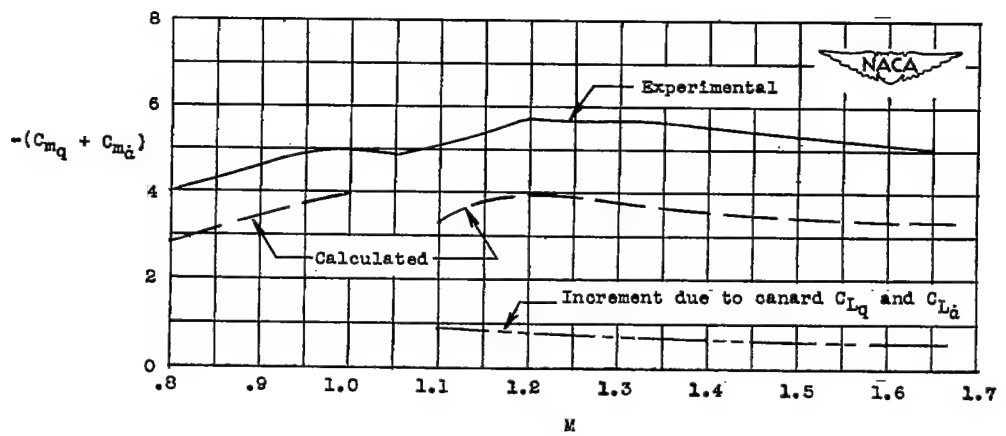

Figure 19.- Geometric characteristics and damping coefficients for a missile configuration having a modified 60° triangular wing and canard surface (model 19).

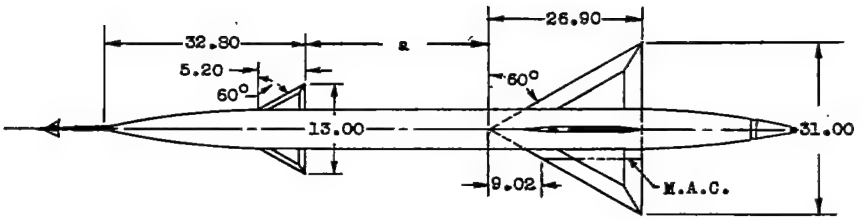

	Model 20	Model 21
Dimension a	29.30	69.30
Dimension b	114.20	154.20
Center-of-gravity station	60.00	91.30

Wing	
A	2.31
S, sq ft	2.835
M.A.C., in.	17.62
Canard	
A	2.31
S, sq ft	.80
M.A.C., in.	7.50

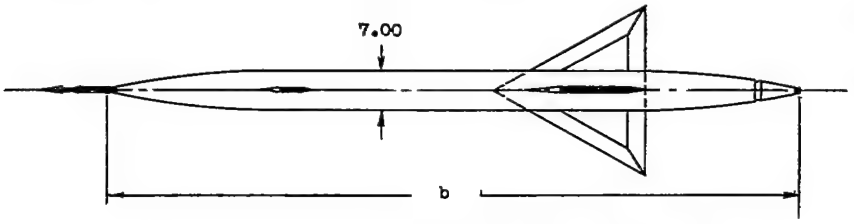

All dimensions are in inches.

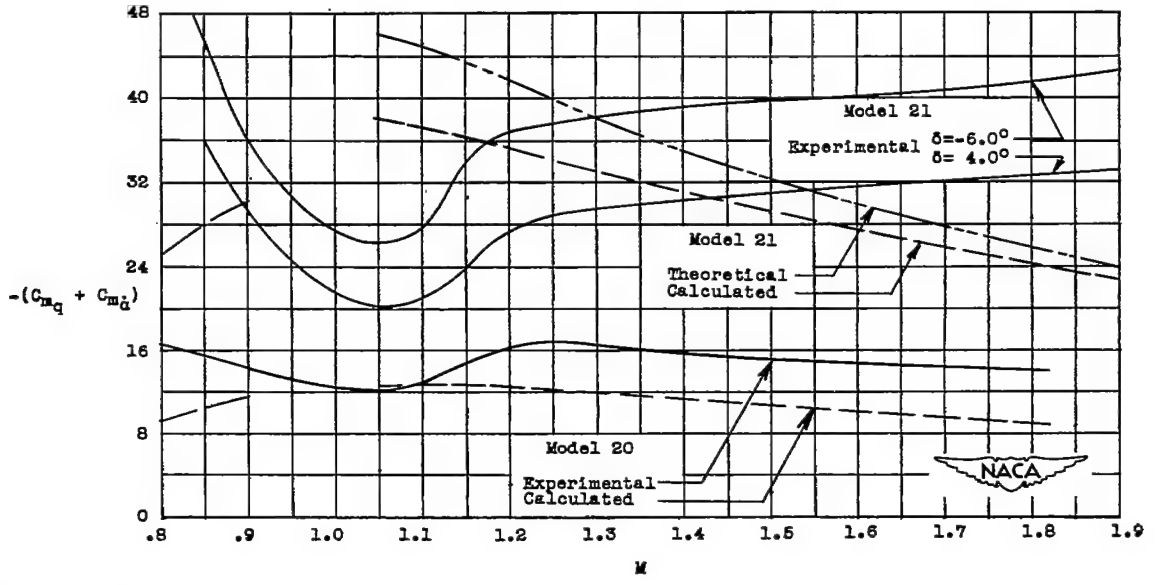

Figure 20.- Geometric characteristics and damping coefficients for two missile configurations having 60° triangular wings and canard surfaces (models 20 and 21).

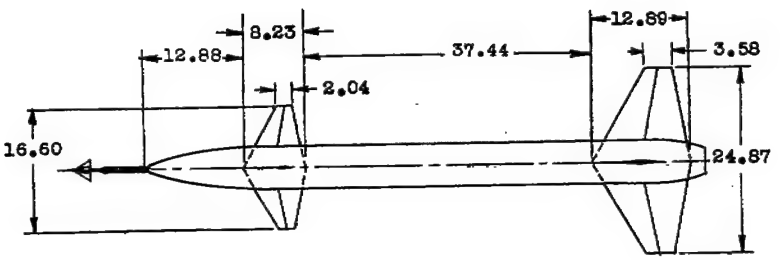

Center-of-gravity location

Model A Station 38.6

Model B Station 40.4

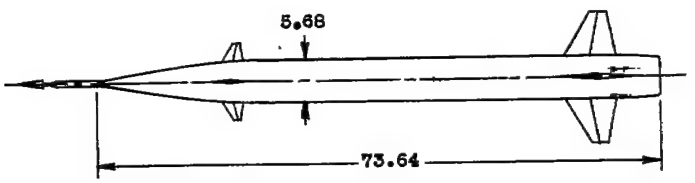

Wing	
A	3.02
S, sq ft	1.422
M.A.C., in.	9.20

Canard	
A	3.24
S, sq ft	.592
M.A.C., in.	5.55

All dimensions are in inches.

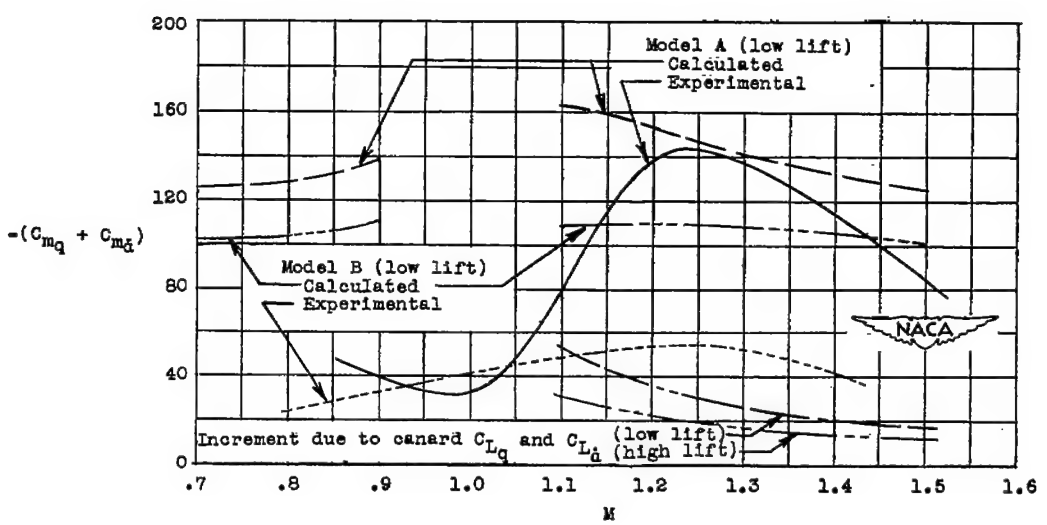

Figure 21.- Geometric characteristics and damping coefficients for a missile configuration having essentially unswept wings and canard surfaces (model 22).

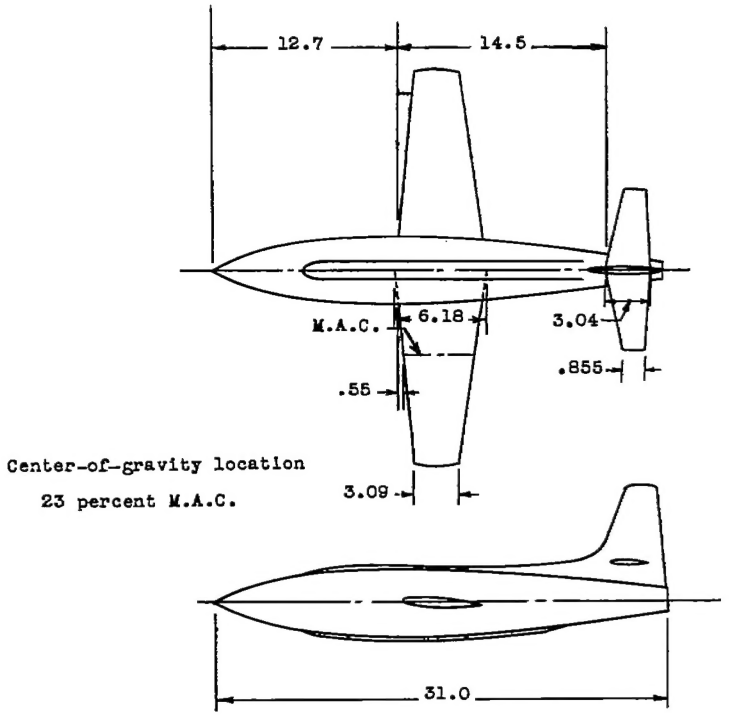

Wing	
A	6.0
S, sq ft	130.0
M.A.C., ft	4.76
Horizontal Tail	
A	5.0
S, sq ft	26.0

All dimensions are in feet.

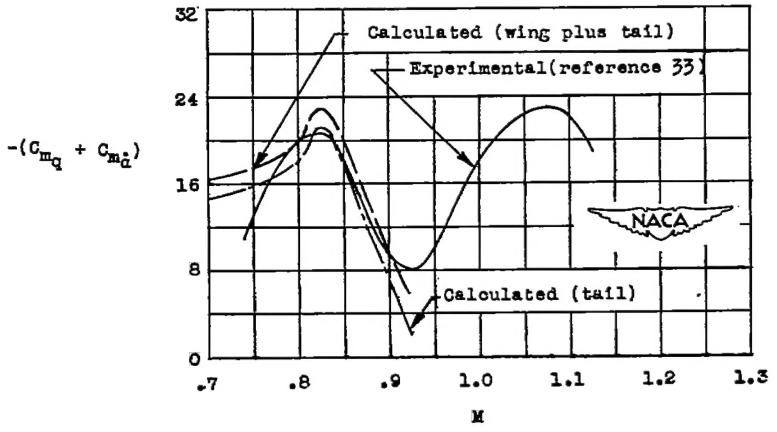

Figure 22.- Geometric characteristics and damping coefficients for the X-1 airplane (airplane 1).

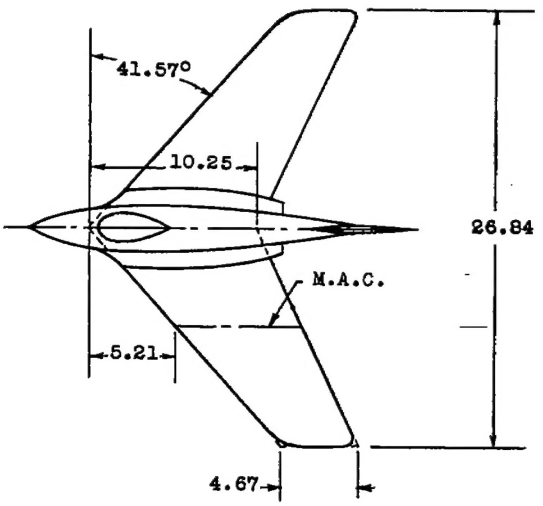

Center-of-gravity location
17.5 percent M.A.C.

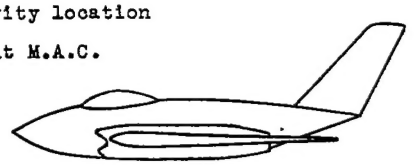

Wing	
A	3.6
S, sq ft	200
M.A.C., ft	7.81

All dimensions are in feet.

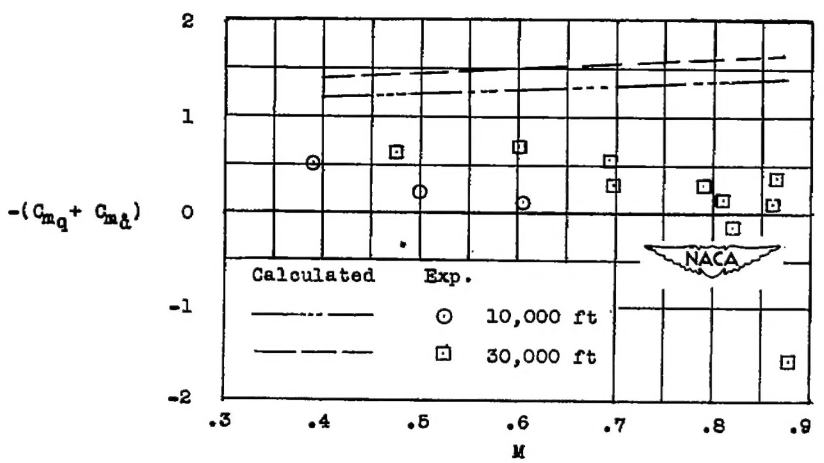

Figure 23.- Geometric characteristics and damping coefficients for the X-4 airplane (airplane 2).

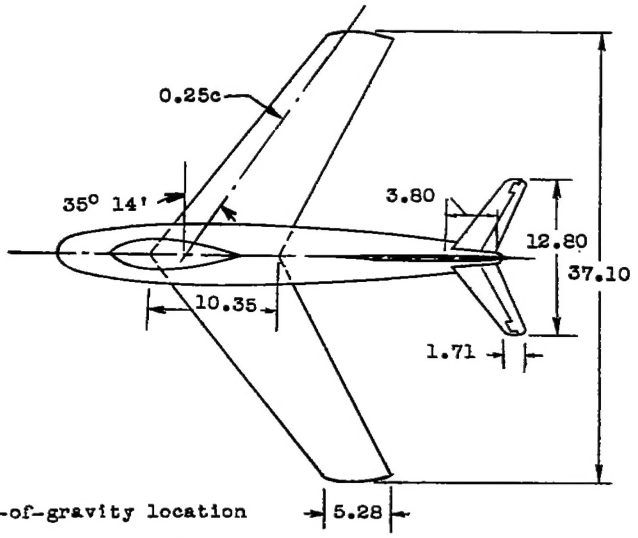

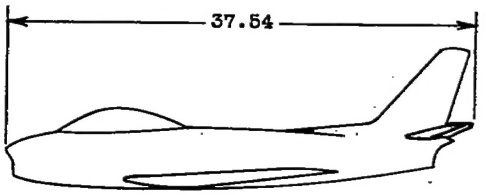

Wing	
A	4.79
S, sq ft	287.9
M.A.C., ft	8.09

Horizontal Tail	
A	4.65
S, sq ft	35.0
M.A.C., ft	2.89
Tail length, ft	18.12

All dimensions are in feet.

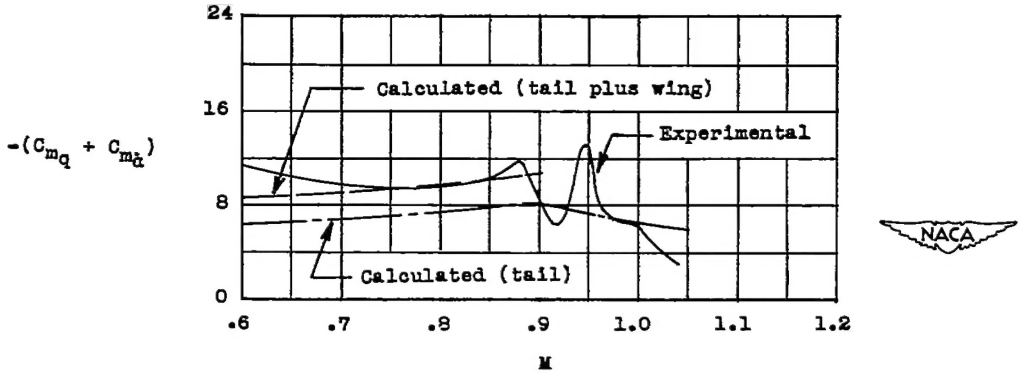

Figure 24.- Geometric characteristics and damping coefficients for the F-86 airplane (airplane 3).

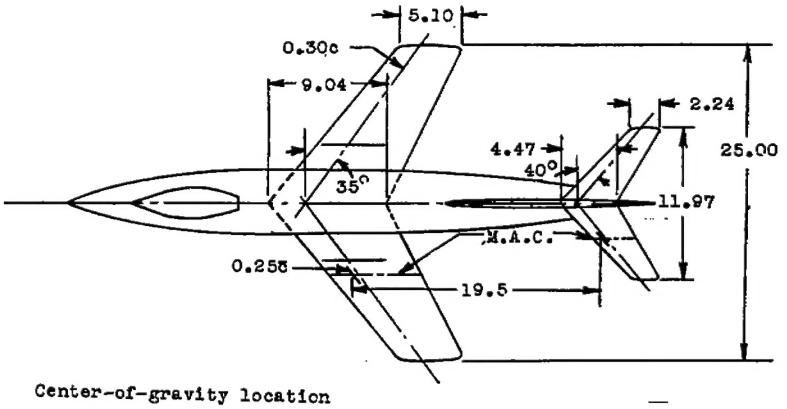

Center-of-gravity location

25.0 percent M.A.C.

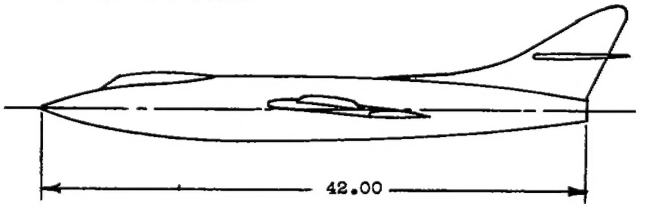

Wing	
A	3.57
S, sq ft	175.0
M.A.C., ft	7.27
Horizontal Tail	
A	3.59
S, sq ft	39.9
M.A.C., ft	3.48

All dimensions are in feet

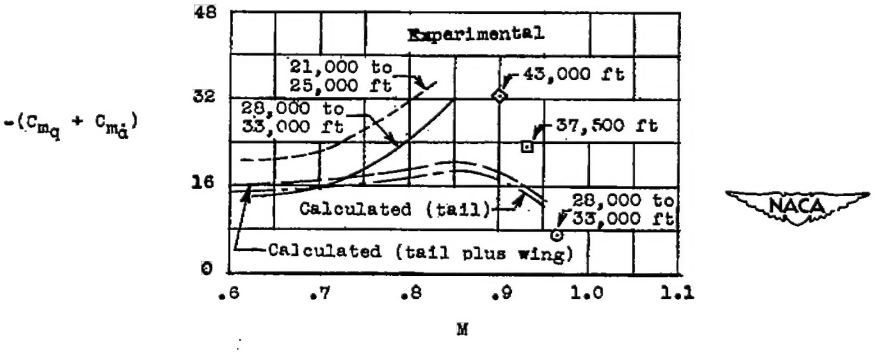

Figure 25.- Geometric characteristics and damping derivatives for the D-558-II airplane (airplane 4).